JCI insight

Cell-autonomous retinoic acid receptor signaling has stage-specific effects on mouse enteric nervous system

Tao Gao, … , Jessica B. Anderson, Robert O. Heuckeroth

JCI Insight. 2021. https://doi.org/10.1172/jci.insight.145854.

Research In-Press Preview **Gastroenterology**

Retinoic acid (RA) signaling is essential for enteric nervous system (ENS) development since vitamin A deficiency or mutations in RA signaling profoundly reduce bowel colonization by ENS precursors. These RA effects could occur because of RA activity within the ENS lineage or via RA activity in other cell types. To define cell-autonomous roles for retinoid signaling within the ENS lineage at distinct developmental time points, we activated a potent floxed dominant-negative RA receptor α (RaraDN) in the ENS using diverse CRE recombinase-expressing mouse lines. This strategy enabled us to block RA signaling at pre-migratory, migratory, and post-migratory stages for ENS precursors. We found that cell-autonomous loss of retinoic acid receptor (RAR) signaling dramatically affects ENS development. CRE activation of RaraDN expression at pre-migratory or migratory stages caused severe intestinal aganglionosis, but at later stages, RaraDN induced a broad range of phenotypes including hypoganglionosis, submucosal plexus loss, and abnormal neural differentiation. RNA-sequencing highlighted distinct RA-regulated gene sets at different developmental stages. These studies show complicated context-dependent RA-mediated regulation of ENS development.

Cell-autonomous retinoic acid receptor signaling has stage-specific effects on mouse enteric nervous system

Tao Gao[1], Elizabeth C. Wright-Jin[2], Rajarshi Sengupta[1], Jessica B. Anderson[1], and Robert O. Heuckeroth[1, 2, 3]*

[1]*Children's Hospital of Philadelphia Research Institute, Philadelphia, PA, USA*

[2]*Department of Pediatrics, Washington University School of Medicine, St. Louis, MO, USA*

[3]*Department of Pediatrics, Perelman School of Medicine at the University of Pennsylvania, Philadelphia, PA, USA*

Present affiliation and location:

Rajarshi Sengupta: American Association for Cancer Research

Elizabeth C. Wright-Jin: Department of Neurology, Nemours, Alfred I. Dupont Hospital for Children

***Corresponding author:**

Robert O. Heuckeroth MD PhD

Professor of Pediatrics

Professor of Cell and Developmental Biology

Irma and Norman Braman Endowed Chair for Research in Pediatric GI Motility Disorders

The Children's Hospital of Philadelphia, Research Institute

3615 Civic Center Blvd

Abramson Research Center – Suite # 1116I

Philadelphia, PA 19104-4318

Email: HeuckerothR@chop.edu Phone: 215-590-1209

Conflict of Interest Statement: Robert O. Heuckeroth is a consultant for BlueRock Therapeutics and served on a Scientific Advisory Board to Takeda.

Abstract

Retinoic acid (RA) signaling is essential for enteric nervous system (ENS) development since vitamin A deficiency or mutations in RA signaling profoundly reduce bowel colonization by ENS precursors. These RA effects could occur because of RA activity within the ENS lineage or via RA activity in other cell types. To define cell-autonomous roles for retinoid signaling within the ENS lineage at distinct developmental time points, we activated a potent floxed dominant-negative RA receptor α (Rarα DN) in the ENS using diverse CRE recombinase-expressing mouse lines. This strategy enabled us to block RA signaling at pre-migratory, migratory, and post-migratory stages for ENS precursors. We found that cell-autonomous loss of retinoic acid receptor (RAR) signaling dramatically affects ENS development. CRE activation of Rarα DN expression at pre-migratory or migratory stages caused severe intestinal aganglionosis, but at later stages, Rarα DN induced a broad range of phenotypes including hypoganglionosis, submucosal plexus loss, and abnormal neural differentiation. RNA-sequencing highlighted distinct RA-regulated gene sets at different developmental stages. These studies show complicated context-dependent RA-mediated regulation of ENS development.

Introduction

The enteric nervous system (ENS) is a complex network of neurons and glia that resides in the bowel wall and is essential for intestinal function (1, 2). These ENS cells arise primarily from vagal enteric neural crest-derived cell (ENCDC) precursors that divide rapidly and colonize the bowel in a rostral to caudal direction from E9 to E13.5 in mice (3-6). In addition to vagal ENCDC, ENS precursors include sacral neural crest (7), mesenteric neural crest (8), sympatho-enteric precursors (9), Schwann cells (10) and perhaps bowel epithelial cells (11). As ENCDC colonize the bowel they differentiate into ~20 neuron types and many types of glia that form extensive networks to control most aspects of bowel function (2, 12-17). Maturation of the ENS continues during fetal development and remodeling continues after birth (18-20). Retinoic acid (RA), the active metabolite of vitamin A, is an important morphogen with an integral role in ENCDC migration, proliferation, and differentiation (21-33). RA functions mainly as a transcriptional regulator that binds to and activates retinoic acid receptor (RAR)/retinoid x receptor (RXR) heterodimers (34). RAR/RXR bind DNA at retinoic acid response elements (RAREs) to regulate transcriptional activity. Several studies demonstrate vital roles for vitamin A and its active metabolite RA in ENS development. In rat and mouse primary cell culture, RA increases enteric neural crest-derived cell (ENCDC) proliferation and neuronal differentiation while decreasing neurite length (23, 27). *In vivo*, vitamin A deficient mice (*Rbp4*$^{-/-}$ mice on a vitamin A deficient diet) develop distal bowel aganglionosis (26), confirming vitamin A is needed for bowel colonization by ENCDC. The extent of bowel aganglionosis dramatically increased when *Ret* heterozygosity was combined with vitamin A deficiency suggesting potent gene-environment interactions in mice (26, 35). Consistent with these observations, loss of the primary RA synthesis enzyme retinaldehyde dehydrogenase 2 (*Raldh2*) also causes severe intestinal aganglionosis in mice (30), with more minor effects of murine *Raldh1* and *Raldh3* mutations (25). Furthermore, maternal vitamin A deficiency or excess can cause intestinal hypoganglionosis without aganglionosis in rats and mice

(22, 29, 33). While these results clearly show RA signaling is needed for ENS development, many questions remain. First, because RAR and RXR receptors are expressed in diverse cell types (27) it is not clear whether RA acts directly on ENCDC or via effects on neighboring cells. Second, effects of RA signaling at distinct developmental stages remain elusive. Third, the RA-targeted gene network in ENCDC *in vivo* is not yet established. To address these questions, we employed a very potent CRE-dependent dominant negative retinoic acid receptor alpha (36) in combination with fluorescence-based lineage tracing in mice. We discovered that RA signaling regulates ENS development in a cell-autonomous manner, with distinct effects on different developmental stages. Furthermore, gene expression profiling showed stage-specific effects of blocking RAR signaling in developing ENCDC. These results suggest that vitamin A deficiency or excess could alter ENS structure and function in many ways during intrauterine and postnatal periods, contributing to human bowel motility disorders.

Results

Cell-autonomous RAR signaling in neural crest derivatives is required for craniofacial and ocular development

To characterize cell-autonomous roles for RAR signaling within the ENS lineage, we bred *RarαDN$^{LoxP/+}$* to *Wnt1Cre*+ mice. *RarαDN$^{LoxP/+}$* produce a dominant negative retinoic acid receptor (RARαDN) after CRE-mediated DNA recombination. *Wnt1Cre* express *Cre* recombinase in the central nervous system and many neural crest derivatives including essentially all fetal ENS precursors (37-39). *RarαDN$^{LoxP/+}$; Wnt1Cre*+ mice are viable at E12.5, but die by E14.5 (Table 1). E12.5 *RarαDN$^{LoxP/+}$; Wnt1Cre*+ have major malformations of neural crest-derived facial structures (Figure 1A, B) with absent facial cartilage (Figure 1C, D). Sectioning showed failure of nasomedial process fusion at the midline and a wide frontonasal region (Figure 1E, F). In contrast, dorsal root ganglia (DRG), another crest-derived structure, appeared fairly normal even though *Wnt1Cre* induced recombination of an EYFP reporter in DRG (Figure 1G-L). These data highlight distinct RA roles in different neural crest-derived tissues during development. Our primary goal was to investigate RA signaling effects in the ENS.

ENS development requires cell autonomous RAR signaling

At E12.5 in *Wnt1Cre*+ (control) mice, ENCDC had colonized the esophagus, stomach, small intestine and half of the colon, as seen by TuJ1 (neuron specific beta 3 tubulin) antibody staining (Figure 2A). In contrast, E12.5 *RarαDN$^{LoxP/+}$; Wnt1Cre*+ mice only had TuJ1^{+} cells in the esophagus and stomach (Figure 2B). Recognizing that the absence of TuJ1 staining might reflect impaired neuronal differentiation in *RarαDN$^{LoxP/+}$; Wnt1Cre*+ mice or could reflect absent ENS, we bred to *R26R-TdTomato* lineage reporter mice so that cells undergoing CRE-mediated DNA recombination are unambiguously marked. While TdTomato+ ENS and HuC/D+ (neuronal RNA binding protein) neurons were readily detected in stomach, small bowel and proximal colon of

control animals (Figure 2C-E, I), the *RarαDN$^{LoxP/+}$; Wnt1Cre+; R26R-TdTomato*+ mice did not have TdTomato+ or HuC/D+ cells in the small bowel or colon and had fewer ENS cells in stomach than controls (Figure 2F-H, J). These analyses confirmed that blocking cell-autonomous RAR signaling in the *Wnt1Cre* lineage completely prevented these ENS precursors from colonizing small bowel and colon.

Blocking RAR signaling causes defects in ENCDC migration and differentiation by E10.5

To determine if *RarαDN* expression within neural crest-derived ENS precursors acts at earlier developmental stages, we examined E10.5 whole embryo via 3DISCO tissue clearing (40) and confocal microscopy (Figure 3 A, B). TuJ1 and SOX10 antibody staining showed many ENCDC in esophagus and stomach in control mice (Figure 3C-F), but very few stained ENCDC in proximal bowel of *RarαDN$^{LoxP/+}$; Wnt1Cre*+ mice (Figure 3G-J), consistent with a defect in early stages of bowel colonization. More specifically, while there were some SOX10+ ENCDC near the vagus in mutant mice (Figure 3G-J), the control mice had many SOX10+ ENCDC that had migrated far beyond the vagus and into the stomach (Figure 3C-F). Furthermore, in control mice, many ENCDC were TuJ1 immunoreactive, suggesting early neuronal differentiation (Figure 3C, E), but there were almost no TuJ1+ cells in the esophagus or stomach of *RarαDN$^{LoxP/+}$; Wnt1Cre*+ mice (Figure 3G, I). Collectively these data suggest cell-autonomous RAR signaling is needed for ENCDC to populate the bowel and differentiate into neurons.

Cell autonomous RAR signaling is required for RET and PHOX2B expression in ENCDC

The defect in bowel colonization by ENCDC of *RarαDN$^{LoxP/+}$; Wnt1Cre*+ mice closely resembles the phenotype in *Ret* and *Phox2b* null mice (41, 42) (Figure 4A-C). Because retinoic acid was previously reported to induce *Ret* expression in quail ENCDC migrating from neural tube to bowel (24), we stained E12.5 bowel from *RarαDN$^{LoxP/+}$; Wnt1Cre+; R26R-EYFP*+ and controls

(*Wnt1Cre+; R26R-EYFP+*) with RET antibody. 100% of stomach EYFP+ ENCDC expressed RET in controls as expected (Figure 4D-F). Curiously, while one *RarαDN$^{LoxP/+}$; Wnt1Cre+; EYFP+* mouse had many RET+ EYFP+ ENCDC in stomach (42%), the other mice evaluated had very few RET+ EYFP+ ENCDC (0%, 0%, 0.4%, and 4.9%) (Figure 4G-I, J). RARαDN also dramatically reduced the percentage of lineage-marked ENCDC that express PHOX2B in stomach or esophagus of *RarαDN$^{LoxP/+}$; Wnt1Cre+; TdTomato* mice (Figure 5A-F, H). EdU incorporation into lineage marked ENCDC in E12.5 stomach of *RarαDN$^{LoxP/+}$; Wnt1Cre+; TdTomato* mice, however, was not statistically different from controls (Figure 5A-F, G) so it is not clear that reduced proliferation within stomach ENCDC fully accounts for the phenotype. Collectively these data suggest RAR signaling is needed in the *Wnt1Cre* ENS lineage for *Ret* and *Phox2b* expression, suggesting that loss of either RET or PHOX2B could cause this type of extensive intestinal aganglionosis (41, 42).

Loss of RAR signaling causes defective vagal nerve development

In parallel with the loss of ENCDC in fetal stomach, E11.5 *RarαDN$^{LoxP/+}$; Wnt1Cre+* mice had smaller vagus nerves than control littermates (Figure 6 A-C). The reduction in vagal nerve fibers in the stomach appears to be non-cell autonomous because TuJ1+ vagal nerve fibers are TdTomato negative in *Wnt1Cre+; TdTomato+* and *RarαDN+; Wnt1Cre+; TdTomato+* mice (Figure 6D, Supplemental Figure 1, Supplemental Videos 1 and 2). Enlarged images also demonstrate many TdTomato+ cells migrating along the TuJ1+ vagal nerve fibers in *Wnt1Cre+; TdTomato* and *RarαDN; Wnt1Cre+; TdTomato* mice (Supplemental Figure 1E, F, K, L). Furthermore, while ENCDC migrate far beyond the vagus in control animals, TuJ1$^+$ and SOX10 labeled ENCDC remained close to vagal fibers in E11.5 *RarαDN$^{LoxP/+}$; Wnt1Cre+* mice (Figures 3D, H and 6 A, B). These observations suggest synergistic interactions between growing vagal nerve fibers and migrating ENCDC that colonize the bowel to form ENS.

Loss of RAR signaling in SOX10 lineage of ENCDC causes aganglionosis.

To evaluate cell-autonomous effects of RAR beyond E12.5 when *RarαDN$^{LoxP/+}$; Wnt1Cre*+ die, we generated *RarαDN$^{LoxP/+}$; SOX10Cre*+ mice. These mice express *Cre* from *Sox10* regulatory elements beginning at E8.5 when ENCDC migrate through the paraxial mesoderm to foregut (43). To confirm CRE activation in the ENS lineage, we examined *SOX10Cre; R26R-TdTomato* mice at E12.5 and found essentially complete overlap of the TdTomato lineage marker and RET antibody staining in the bowel (Supplemental Figure 2). Like *RarαDN$^{LoxP/+}$; Wnt1Cre*+, the E12.5 *RarαDN$^{LoxP/+}$; SOX10Cre*+ had TuJ1^{+} ENCDC predominantly confined to the stomach at E12.5 (Figure 7 B-E), with a few sparsely distributed TuJ1^{+} ENCDC in proximal small intestine (Figure 7D). By E15.5, *RarαDN$^{LoxP/+}$; SOX10Cre*+ had obvious eye and craniofacial defects but remained viable (Figure 7F). The E15.5 ENS network was dense in esophagus and stomach, but sparse in proximal small intestine (Figure 7G, J, L, N) compared to controls (Figure 7I, K, M,). Distal small intestine and colon were aganglionic with extrinsic nerve fibers in distal colon (Figure 7H, R). Neurons in the small bowel were often associated with extrinsic nerve fibers and separated from more proximal ENS (Figure 7S-V). These data are consistent with the hypothesis that RAR signaling is required as ENCDC migrate from neural tube to bowel and is not needed by ENS precursors before E8.5 in the neural tube.

Blocking RAR signaling in the TyrCre* lineage *reduces enteric neurons and alters ENS patterning

We next examined the ENS in mice that express *Cre* in ENCDC from the tyrosinase promoter (*RarαDN$^{LoxP/+}$; TyrCre*+) starting at E10.5 (43, 44) when ENCDC normally reach the midgut (3). In these mice, the extent of bowel colonization by ENCDC was similar to controls at E13.5 (Figure 8A, E). Stomach ENS appeared normal in *RarαDN$^{LoxP/+}$; TyrCre*+ mice (Figure 8B, F), but the

small bowel and colon were hypoganglionic relative to controls (Figure 8C, D, G, H). ENS organization was also abnormal in the small bowel and colon of mutants at E13.5. Instead of the fine network of cells seen in controls, *RarαDN$^{LoxP/+}$; TyrCre*+ ENS had thick chains of cells (Figure 8A, C-E, G, H). At birth, *RarαDN$^{LoxP/+}$; TyrCre*+ mice appeared healthy, but do not feed (absent milk spot) (Figure 8I) and consistently die within 12 hours (n = 6). To avoid analysis of dying mice, we examined E18.5 ENS. Although the *RarαDN$^{LoxP/+}$; TyrCre+; R26R-TdTomato* bowel looked grossly normal (Figure 8J), lineage-marked TdTomato+ ENS cells were less dense in mutant bowel throughout the small intestine and colon (Figure 8K). HuC/D immunohistochemistry confirmed enteric neurons were sparse (Figure 8L, N-P) and that all neurons in *RarαDN$^{LoxP/+}$; TyrCre+; R26R-TdTomato* bowel were TdTomato positive (Figure 8L, M). To determine if blocking RAR impacted neuron subtype ratios, we counted NOS1 and HuC/D double labeled cells and discovered more HuC/D+ neurons were NOS1+ in *RarαDN$^{LoxP/+}$; TyrCre*+ ENS (Figure 8Q-S) compared to controls. Collectively these results show cell-autonomous RAR signaling is important after E10.5 for ENS patterning, to increase neuron number, and for neuron subtype specification.

Inactivation of RAR signaling in RET lineage causes distal bowel hypoganglionosis

Sparse ENS in the preceding models might reflect inadequate RET making it difficult to identify other roles for RAR signaling in ENCDC. Our prior studies suggested RA is not needed to sustain *Ret* expression in ENCDC that already express *Ret* (26). We therefore decided to use mice expressing *CRE-ERT2* from the *Ret* locus to activate *RarαDN* expression in ENCDC that already express *Ret*. For these experiments, we also needed a CRE-dependent fluorescent reporter (EYFP) to track CRE activity. Because *Ret* is on mouse chromosome 6 near the *ROSA26* locus that drives expression of *RarαDN* as well as most fluorescent reporters, we bred *RarαDN$^{LoxP/+}$* mice to *RETCreERT2-EYFP^{Tandem}* mice to generate *RarαDN$^{LoxP/+}$; RETCreERT2-EYFP^{Tandem}* and *RarαDN$^{LoxP/+}$* controls. The *RarαDN$^{LoxP/+}$; RETCreERT2-EYFP^{Tandem}* have undergone

recombination so *RETCre-ERT2* and a CRE-activated EYFP-Channelrhodopsin-2 protein are on the same chromosome. E13.5 control *RarαDN$^{LoxP/+}$* lacking CreERT2 had bowel fully colonized by ENS precursors after E10.5 tamoxifen treatment (Figure 9A, B, D, F, H). E10.5 tamoxifen treated *RarαDN$^{LoxP/+}$; RETCreERT2-EYFP^{Tandem}* also had normally patterned ENS in the small bowel (Figure 9A, C, G) but hypoganglionic ENS in the colon with thick chains of ENS cells (Figure 9C, I). We confirmed high levels of CRE-activation in the ENS after tamoxifen treatment and almost no CRE activation in the absence of tamoxifen in these *RETCreERT2-EYFP^{Tandem}* mice (Supplemental Figure 3). Because tamoxifen effects may take 12-18 hours, we also tamoxifen treated at E8.5 but found similar phenotypes (Figure 9J-M). RET and PHOX2B were readily detected in EYFP+ ENCDC of E13.5 *RarαDN$^{LoxP/+}$; RETCreERT2-EYFP^{Tandem}* mice, consistent with our prior studies (26, 27). These data suggest RAR is needed to activate RET and PHOX2B expression in ENCDC (Figures 4D-I, 5A-F, H) but not to maintain expression once regulatory elements are activated (Figure 9N-Q). The unusual patterning in distal colon of tamoxifen-treated E13.5 *RarαDN$^{LoxP/+}$; RETCreERT2-EYFP^{Tandem}* mice suggests that RAR regulates additional ENS patterning genes in ENCDC.

Ret lineage loss of RAR signaling profoundly reduced submucosal neuron density and altered cell identity

RarαDN$^{LoxP/+}$; RETCreERT2-EYFP^{Tandem} treated with tamoxifen at E10.5 (Figure 10) were born at a normal Mendelian ratio, grew normally, and had a normal appearing colon (Figure 10B) permitting analysis of adult ENS. We therefore stained the bowel of two month old mice with HuC/D and TuJ1 antibodies (Figure 10C-N). Quantitative analysis demonstrated a 50-65% reduction in myenteric neurons in small bowel and colon and a 90% loss of submucosal neurons in *RarαDN*-expressing mutant mice (Figure 10O-T). In contrast to neurons, adult enteric glia marked by SOX10 antibody appeared similar in abundance in tamoxifen-treated

RarαDN$^{LoxP/+}$; RETCreERT2-EYFP^{Tandem} and control mice (Supplemental Figure 4A). Interestingly, E10.5 tamoxifen treatment also led to a dramatic increase in NOS1+ submucosal neurons in *RarαDN$^{LoxP/+}$; RETCreERT2-EYFP^{Tandem}* small bowel (Supplemental Figure 4B), and a mild increase in NOS1+ myenteric neurons. These studies confirm distinct age-dependent effects of cell-autonomous RAR signaling in the ENS.

Transcriptional profiling shows RARαDN differentially impacts gene expression in E11.5 stomach and E13.5 colon ENCDC

Because RAR regulates transcription, we performed pooled-cell RNAseq to characterize RARαDN-induced changes in ENCDC gene expression. For *RaraDN$^{LoxP/+}$; Wnt1Cre+; R26R-TdTomato* mice, we analyzed E11.5 stomach ENCDC because RARαDN eliminated ENCDC beyond the stomach. For *RarαDN$^{LoxP/+}$; RETCreERT2-EYFP^{Tandem}*, we analyzed E13.5 colon ENCDC after tamoxifen treatment at E10.5 because RARαDN-expressing colon ENCDC had patterning defects. Controls expressed fluorescent protein in ENCDC, but lacked *RarαDN*. Flow sorting cleanly separated fluorescent cells from other bowel cell types (Figure 11A, B). Multidimensional scaling showed separate groups of control versus *RarαDN*-expressing ENCDC (Figure 11C, D). Among ~ 23,000 transcripts at each age, we found 1413 genes differentially-expressed between control and *RaraDN$^{LoxP/+}$; Wnt1Cre+* ENCDC (FDR < 0.05) at E11.5 (Supplemental Table 1) and 1140 genes differentially-expressed between control and *RaraDN$^{LoxP/+}$; RETCreERT2-EYFP^{Tandem}* (FDR < 0.05) at E 13.5 (Supplemental Table 2) as represented in Volcano plots (Figure 11E, F). The top 20 upregulated and downregulated genes at E11.5 (Supplemental Figure 5A) and E13.5 (Supplemental Figure 5B) and main dysregulated pathways (Figure 12A for E11.5 and Figure 12B for E13.5) suggest many distinct biological processes are influenced by RAR signaling.

One initially surprising feature at E13.5 was that many hemoglobin genes were less abundant in flow sorted cells from *RarαDN; RETCreERT2-EYFP^{Tandem}* compared to controls. We suspect that this occurred because *Ret* is expressed in the hematopoietic stem cell (HSC) lineage where RAR supports erythropoiesis (45, 46) and hemoglobin genes are normally expressed at high levels. Consistent with this hypothesis, some *RETCre-ERT2-EYFP^{Tandem}*-lineage cells in the colon were stained with TER119 (erythroid lineage) and CD31 (endothelial, platelet and leucocyte lineage) antibodies (Supplemental Figure 6). To define a gene set clearly linked to the ENS, we compared differentially expressed genes in *RarαDN; RETCreERT2-EYFP^{Tandem}* and *RarαDN; Wnt1Cre; TdTomato* mice. 594 genes were differentially regulated versus age-matched control cells in both mouse lines (Supplemental Figure 7 and Supplemental Table 3). Of these, a core set of 115 genes were regulated in the same direction by RARαDN in ENCDC at E11.5 and E13.5 (Supplemental Tables 4 and 5). Gene enrichment pathway analysis of the aforementioned two sets of genes showed many pathways related to neuron development (Supplemental Figure 7). To validate RNAseq data, we selected two differentially expressed genes of ENCDC at E11.5 (*Stmn2* and *Pax3*) and performed quantitative reverse transcriptase PCR (qRT-PCR), which confirmed differences predicted by RNA sequencing (Supplemental Figure 8). The RNAseq data for *Ret* and *Phox2B* in E11.5 stomach also correlate well with our immunohistochemistry for RET and PHOX2B protein (Figure 4, Figure 5, Supplemental Figure 9).

Discussion

Retinoic acid regulates activity of the RAR/RXR transcription factor family to alter gene expression and influence many aspects of development (34). Prior studies using constitutive knockout mice, RAR antagonist, stem cells or vitamin A depletion in mice and rats show critical roles for RA in the developing ENS (21, 23-29, 31-33). For example, loss of the RA biosynthetic enzyme retinaldehyde dehydrogenase 2 (RALDH2) causes extensive bowel aganglionosis in *Raldh2-/-* mice (28), while *Raldh1-/-* and *Raldh3-/-* mice have milder ENS defects (25). The *Raldh2-/-* phenotype probably occurs because RA is needed in vagal paraxial mesoderm starting at E9 in mice (or E1.5 in avians) to induce *Ret* expression in ENCDC as these cells migrate from neural tube to bowel (24). In contrast, when RAR signaling was blocked by the chemical pan-RAR antagonist BMS493 at E11.5 in organ culture (26) or at E12.5 in dissociated cell culture (27), RET expression in ENCDC appeared unaffected by RAR inhibition. Nonetheless, RAR inhibition at these later stages impaired ENCDC proliferation, bowel colonization, neurite growth, neuronal differentiation, and ENS patterning (23, 26, 27). Consistent with these observations, nutritional deficiency in the retinoic acid precursor vitamin A causes distal bowel aganglionosis in mice, mimicking human Hirschsprung disease (HSCR) (26) and gene variants in people with HSCR may alter RA signaling (47, 48). These studies suggest that RA signaling could impact ENS development in many ways depending on the timing and severity of the RA signaling defect.

Prior strategies did not define the cell types influenced by RA signaling. To determine how cell-autonomous RAR signaling affects the ENS lineage, we used a potent CRE-inducible dominant negative RAR transgene (RARaT403) that blocks all three RAR receptors (i.e., *RarαDN$^{LoxP/+}$* mice) (49). By breeding to several different CRE-expressing mouse lines, we induced RARaT403 (RARαDN) expression selectively within ENCDC at specific times during development. Our *RarαDN$^{LoxP/+}$; Wnt1Cre+* studies show that cell-autonomous RAR signaling

within ENCDC is required to activate *Ret* expression early in development, consistent with data from zebrafish (21) and avian models (24). RAR signaling is also needed to activate *Ret* in ureteric bud suggesting similar cell-autonomous mechanisms may control *Ret* expression in kidney and developing ENS (36, 50). In contrast, when CRE expression is driven by *Ret* regulatory elements, *RarαDN* induction did not lead to loss of RET protein in ENCDC, suggesting RA is needed to turn on *Ret*, but not to maintain *Ret* expression, consistent with our prior BMS493 data (26, 27). We were surprised to discover that PHOX2B protein was also undetectable in ENCDC of *RarαDN$^{LoxP/+}$; Wnt1Cre+* mice. Loss of PHOX2B could, by itself, explain the loss of RET in *RarαDN$^{LoxP/+}$; Wnt1Cre+* ENCDC (42), but we are unable to find evidence that PHOX2B regulates RET in the kidney suggesting that *Ret* is regulated by RA via additional PHOX2B-independent mechanisms as supported by prior studies (31, 47, 51).

There were many other interesting observations. First, the thick chains of enteric neurons seen in distal bowel of *RaraDN$^{LoxP/+}$;* TyrCre+ and *RaraDN$^{LoxP/+}$; RETCreERT2-EYFP^{Tandem}* mice closely resemble the colon ENS patterning defect we observed in BMS493-treated fetal gut organ cultures (26). This suggests that the normal dispersion of enteric neurons into small colon ganglia is RA dependent. Second, in fetal *RaraDN$^{LoxP/+}$; SOX10Cre+* mice we saw some clustered small bowel enteric neurons near extrinsic nerve fibers, but far from the more proximal ENS cells. These clusters closely resemble Schwann cell-derived ENS described by Uesaka *et al*, but ENCDC we observed were restricted to small regions of fetal bowel (10). Alternatively, these cells might originate from the “mesenteric neural crest cells” recently described by Yu *et al*, which they hypothesize contribute to human skip segment Hirschsprung disease (8) Third, vagus nerves at E11.5 in *RaraDN$^{LoxP/+}$; Wnt1Cre+* mice occupied a smaller area of the stomach than in control animals. Since vagus nerve fibers were not TdTomato labeled in *Wnt1Cre; R26R-TdTomato* mice, this suggests reciprocal interactions between migrating *Wnt1Cre* lineage ENCDC and growing vagal fibers. Fourth, in addition to ~80%

reduction in total neuron number in the ENS of *RaraDN$^{LoxP/+}$; TyrCre+* mice, there was a striking increase in the percentage of enteric neurons that express NOS1 (nitric oxide synthase). We confirmed that these NOS1+ neurons had expressed CRE using an *R26R-TdTomato* reporter. This suggests that NOS1+ neuron differentiation is less dependent on RAR signaling than other neuron subtypes or that RAR turns off *Nos1* expression in some enteric neuron subtypes. Finally, we found an almost complete loss of submucosal neurons in *RaraDN$^{LoxP/+}$; RETCreERT2-EYFP^{Tandem} mice* treated with tamoxifen at E10.5, suggesting a critical role for RA signaling in radial migration of ENCDC to form submucosal plexus. The normal post-natal growth of these tamoxifen-treated *RaraDN$^{LoxP/+}$; RETCreERT2-EYFP^{Tandem} mice* and normal appearance of the adult bowel suggests that loss of ~90% of submucosal neurons is well tolerated, at least in mice. This is interesting in part because we know little about mechanisms controlling radial migration of ENS precursors to the submucosal plexus, with prior studies implicating only GDNF and netrin/DCC signaling in this process (52, 53). These observations highlight the remarkable range of ENS abnormalities that may occur when RAR signaling is inadequate.

One concern is that we did not evaluate ENS biology in every possible control group, so we cannot exclude some effects of tamoxifen, *Cre* alleles, fluorescent reporters, or of the *RarαDN$^{LoxP/+}$* allele in isolation. For example, a recent paper clearly shows that *Wnt1Cre+; R26R-TdTomato+* increases the severity of the *Ednrb-/-* ENS phenotype (8). We therefore encourage readers to carefully review the comparisons we make as they draw conclusions from our data. We also are underpowered to examine the effect of sex on ENS phenotypes, an issue that could be important for some of the milder phenotypes we examined.

One advantage of our strategy is that CRE-dependent expression of RARαDN and a fluorescent reporter in the same cells facilitated flow sorting and RNAseq to identify RAR targets. Our analyses identified thousands of differentially expressed genes in RARαDN-expressing

versus control ENCDC at E11.5 and E13.5 with 115 genes regulated in the same way by RARαDN at each age. Interpreting these data is complicated since RARαDN induces changes in cell type ratios in addition to changes in gene expression in individual cells. Furthermore, it is not clear if the induced changes occur because of direct effects on retinoic acid response elements (RAREs) or if they reflect more global effects on the differentiation state of the sequenced cells. For example, loss of PHOX2B in E11.5 ENCDC should change the expression of many genes, independent of effects on RAR activity.

As one strategy to further define the role of RAR signaling, we narrowed our lists to include only differentially expressed genes (FDR < 0.2) where expression changes in the same direction at E11.5 and E13.5 for RARαDN+ cells (Supplemental Table 4 and 5). At E11.5, there were 55 genes expressed at higher levels in WT ENCDC than in RARαDN+ ENCDC. 35 of these genes had easily identified functions in neurons. 13 genes at E11.5 were more abundant in RARαDN+ ENCDC than in WT ENCDC. This list included *Rest*, an epigenetic master negative regulator of neurogenesis (54, 55) and *Bmp4* a gene with complex roles in ENS patterning (56-63). At E13.5 our list included 44 genes more abundant in WT than in RARαDN+ cells. 29 of these genes had easily identified roles in neurons. Genes more abundant in RARαDN+ than in WT cells at E13.5 included *Rest*, *Sox10* and *Ets1*, consistent with a role for RAR in ENS neurogenesis. The SOX10 transcription factor is essential for ENS development (64) at least in part because SOX10 activates RET expression (65, 66). However, as multipotent ENCDC differentiate into enteric neurons, SOX10 expression is lost, while enteric glia continue to express SOX10 through adulthood (3). ETS1 enhances *Sox10* expression and is essential to make radial glia in *Xenopus* (67). Consistent with these mRNA findings, SOX10+ cells were abundant in myenteric and submucosal plexus of adult *RaraDN*-expressing mice even though *RarαDN$^{LoxP/+}$; RETCreERT2-EYFP^{Tandem}* had a ~90% reduction in submucosal neurons and the enteric glia are derived from RET+ ENCDC (68). In addition, many Wnt ligands (Wnt1, Wnt2, Wnt4, and Wnt10a) were highly

differentially expressed in E11.5 ENCDC of *RaraDN*$^{LoxP/+}$*; Wnt1Cre*+ versus control. Since Wnt signaling plays important roles in many aspects of neural development (69-72), RAR might alter Wnt signaling to regulate ENCDC development. Collectively these data suggest that cell-autonomous RAR signaling directs neurogenesis in the ENS from multipotent ENCDC and that cell-autonomous RAR signaling has distinct effects at many stages of ENS development. Our observations further suggest that maternal retinoid status during pregnancy and post-natal vitamin A deficiency or excess could have long term effects on ENS structure and function. This may be important because vitamin A deficiency is a common problem in many regions of the world (73).

Methods:

Mouse strains

RarαDN$^{Loxp\text{-}STOP\text{-}LoxP/+}$ (previously described (36)) were rederived from sperm into *C57BL/6J* background by the CHOP transgenic core. *H2az2(Tg(Wnt1cre)11Rth* (RRID:2386570_JAX:003829; referred to as *Wnt1Cre*), *TyrCre* (RRID: MGI: 358524_JAX:029788), *SOX10Cre* (MGI:3586900_JAX:025807), *Rosa26^{EYFP}* (*Gt(ROSA)26Sortm1(EYFP)Cos,* (MGI: 2449038, RRID:IMSR_EM:09668)), and *Gt(ROSA)26Sortm9(CAGtdTomato)Hze* (RRID:IMSR_JAX:007909; referred to as *R26R-TdTomato*) were from The Jackson Laboratory (Bar Harbor, ME) and maintained in *C57BL/6J* background. *RETCreERT2-EYFP^{Tandem}* mice, a gift from Dr. Wenqin Luo (University of Pennsylvania, Philadelphia PA, USA), were generated by breeding *RETCreERT2* (RRID: MGI ID: 4437245) to mice with *Channelrhodopsin-2 (ChR2)-Lox-Stop-Lox-EYFP* in the *Rosa26* locus (74). Mouse *Ret* and *Rosa26* locus are close together (~5 million base pairs), but *RETCreERT2-EYFP^{Tandem}* recombined so that they are on the same chromosome. *Ret$^{TGM/TGM}$* (*Ret-/-* null allele *Ret^{tm1Jmi}*) on C57Bl/6J were previously described (75). A complete list of mouse strains is in Supplemental Table 6 Genotyping was performed using previously published and novel primers (Supplemental Table 7.

Mouse husbandry

Mice had a 12 hour light-dark cycle with free access to food and water. Additional details based on ARRIVE guidelines (76) are in Supplemental Table 8 For timed pregnant mating, *RarαDN$^{Loxp\text{-}STOP\text{-}LoxP/+}$* (called *RarαDN*) female mice were bred to *Cre*-expressing males in the late afternoon. Successful mating was confirmed by vaginal plug the next morning, which was designated embryonic day (E) 0.5 (E0.5).

EdU incorporation assay

EdU analyses were performed using a Click-iT EdU imaging kit (ThermoFisher Catalog# C10337). Timed pregnant animals (E12.5) were injected (intraperitoneal) with EdU (12.5 µg/gm body weight). Tissues were dissected 4 hours after EdU and fixed (4% paraformaldehyde (PFA), 30 minutes at room temperature) before staining using manufacturer's protocol.

Whole mouse embryo imaging using 3DISCO clearing

3DISCO imaging was performed as described (9) with modification. Briefly, E10.5 embryos from timed-pregnant females were washed in phosphate buffered saline (PBS, pH 7.4), fixed (4% PFA, 1 hour, room temperature), and then incubated in SOX10 (1:200, Novus Biologicals, Cat# AF2864) and TuJ1 (1:2000 dilution, Covance, Cat#PRB-435P, RRID:AB_2313773) antibodies in 1X PBS with 0.5% triton X-100 (PBST) and 5% normal donkey serum (NDS) (4^{o}C, constant rocking, 72 hours). After washing 4 times (PBS, room temperature, 15 minutes/wash), embryos were incubated in secondary antibodies and Hoechst 33342 for nuclear staining (2 µg/ml, life technologies, Cat# H3570) in PBST with 5% NDS (4^{o}C, overnight) and then washed 4 times (PBS, room temperature, 15 minutes/wash) and subjected to 3DISCO clearing using a series of tetrahydrofuran (Sigma-Aldrich Cat# 401757) incubations (room temperature, 50%, 70%, and then 80% in double distilled water, 60 minutes each, with rocking), followed by incubation in 100% tetrahydrofuran (3 X 20 minutes, room temperature, rocking) (77). Embryos were then incubated overnight in dibenzyl either (Sigma-Aldrich, Cat# 108014-1KG) at room temperature and mounted in dibenzyl ether before confocal imaging.

Immunohistochemistry

For whole mount staining, fetal bowel was fixed as a tube. Adult bowels were opening along mesentery and pinned flat to Sylgard® before fixation. Bowels were fixed with 4% PFA (40

minutes, room temperature, rocking), washed (4 x 10 minutes, PBS, room temperature), blocked (5% NDS in PBST, room temperature, 1 hour), and then incubated overnight (4°C) with primary antibodies in 5% NDS in PBST. Secondary antibody staining, unless otherwise specified, was done by incubating samples in a 1:400 dilution of the appropriate antibody (1 hour, 25°C). All the primary and secondary antibodies are listed in Supplemental table 9

RNA-Seq analyses

E11.5 stomach ENCDC were isolated from *RaraDN$^{LoxP/+}$; Wnt1Cre+; R26R-TdTomato* and *Wnt1Cre+; R26R-TdTomato* (control) mice E13.5 colon ENCDC were isolated from *RarαDN$^{LoxP/+}$; RETCreERT2-EYFP^{Tandem}* or *RETCreERT2-EYFP^{Tandem}* (control) mice after treatment with tamoxifen (oral gavage, 233 mg/kg body weight dissolved in corn oil) at E10.5. Individual E11.5 stomach and E13.5 colon were incubated with collagenase (Sigma Cat# C0130, 0.2 mg/mL) and dispase (Sigma Cat# 494207800, 0.2 mg/mL) in Ham's F12 media (Gibco Cat# 11765054) with 1% bovine serum albumin (37ºC, 5% CO2 incubator, 20 minutes) and then triturated by pipetting up and down 15 times using P1000 pipette tip before passing through a 30 µm strainer (Corning Cat#352340). Cells with TdTomato or EYFP fluorescence were purified by flow sorting (MoFlo Astrios high speed cell sorter, 100 µm nozzle), pelleted by centrifugation (500 x g), washed once with PBS, and frozen immediately at -80ºC until analysis. RNA isolation, library preparation, and RNA-Seq analysis were performed by University of Pennsylvania Next-Generation Sequencing Core. RNA extracted using the GenElute™ Single Cell RNA Purification Kit (Sigma Cat# RNB300) was analyzed on a 2100 Agilent Bioanalyzer using an RNA 6000 Pico Kit (Agilent, Santa Clara, CA, Cat#5067-1513). The libraries were made using the combination of the Clontech (now Takara) SMART (cDNA synthesis and amplification) and Illumina Nextera XT (cDNA to library) kits. Libraries were then single-end sequenced on an Illumina HiSeq 4000, using Sequencer Software RTA: 2.7.7 and HCS: HiSeqCS:HD 3.4.0.38. Reads were aligned to remove repeat sequences and ribosomal RNA reads and then processed using RNA-Seq unified mapper (RUM)

package (78). RUM files were visualized in the TessLA browser for down-stream analyses. Multidimensional scaling (MDS) analysis, volcano plot, and heatmaps were made on R 4.0.2 platform using limma, edgeR, Glimma, gplots, org.Mm.eg.db, and RColorBrewer. We used ggrepel, ggplot2, and reshape to generate Volcano plots and tidyr, gplots, and ggplot2 generate heatmaps. Gene expression pathway analyses were performed using Ingenuity Pathway Analysis (IPA) package (Qiagen) and Metascape Gene Annotation & Analysis Resource (79). Venn diagram was generated using the Draw Venn Diagram software of Bioinformatics & Evolutionary Genomics, VIB / UGent, Belgium. The RNA-Seq raw data have been deposited in the GEO NIH data repository under the accession number GSE165344.

Real time PCR

E11.5 stomach ENCDC of *RarαDN$^{LoxP/+}$; Wnt1Cre+; R26R-TdTomato* and *Wnt1Cre+; R26R-TdTomato* (control) mice were isolated via the same protocol as for RNA-Seq analysis. RNA was purified using PicoPure RNA isolation kit (Arcturus, Cat# KIT0202). cDNA was made by using First-strand cDNA synthesis using superscript II RT kit (Invitrogen, Cat# 18064-022) with OLIGO(DT)12-18 primer (Invitrogen, Cat#18418012). Quantitative real-time reverse transcriptase PCR (qRT-PCR) was performed using SYBR Green qPCR mixture (Sigma, Cat# S4438). All primers have been previously described and listed in Supplemental table 10. Cycle threshold (Ct) values were normalized to *Gapdh* mRNA.

Confocal microscopy

High-resolution three dimensional images were acquired with a Zeiss LSM 710 confocal microscope using Zeiss ZEN 2.3 SP1 FP3 (black) (Version 14.0.18.201; Zeiss, Oberkochen, Germany) software and a 20x/0.8 air or 63x/1.4 oil DIC M27 Plan-Apochromat objective, except for whole bowel E12.5 and E13.5 imaging, which employed a 5X objective and the ZEN Tile Scan function. Image stitching employed ZEN software. Z-stacks were created with ImageJ/FIJI.

Increments between each slice was 1 μm except for scanning the whole E10.5 embryo, where increments between slices were 3 μm. Videos of Z-stacks were created with the animation function of Imaris 9.02.

Image analysis

Early embryonic, perinatal, and adult mouse bowel cell counting used > 5 randomly-selected x20 fields per animal in each region and FIJI CellCounter module (NIH). Investigators were blinded to genotype when comparing *RarαDN* mutant to controls mice.

Statistics

All experiments include at least three replicates. Statistical analyses employed GraphPad Prism 7 software. Data normality analyses employed the Shapiro-Wilk test. Comparisons between groups used 2-tailed unpaired Student's t-tests. P value < 0.05 is considered statistically significant. Data show mean ± standard error of the mean (SEM).

Study approval

Mouse studies were performed with approval from the Institutional Use and Care Committee at The Children's Hospital of Philadelphia (CHOP) Research Institute (IAC 19-001041) and the Animal Studies Committee of Washington University School of Medicine in St. Louis (#20120130).

Author contributions:

TG and ROH led this study and wrote the manuscript. TG, EWJ, RS, JBA, and ROH designed research studies, conducted experiments, acquired data, analyzed data, and edited the manuscript.

Acknowledgments

We thank Dr. Cathy L. Mendelsohn (Columbia University) for generously sharing her *RarαDN*$^{LoxP/+}$ mice and her insight into retinoid biology. This work was supported by the Irma and Norman Braman Endowment (to ROH), the Suzi and Scott Lustgarten Center Endowment (to ROH), the Children's Hospital of Philadelphia Research Institute (to ROH), Children's Discovery Institute of Washington University and Saint Louis Children's Hospital (MD-II2013-269) (to ROH), and R01 DK087715 (to ROH), March of Dimes 6-FY15-235 (to ROH), and the Burroughs Wellcome Fund Clinical Scientist Award in Translational Research (1008525) (to ROH). We greatly appreciate insightful discussions with Dr. Paul Trainor. We thank the CHOP Flow Cytometry Core and Next-Generation Sequencing Core at The University of Pennsylvania for assisting us with the RNA-Seq experiment. CHOP Transgenic Core helped us re-derive the *RarαDN* mice.

References

1. Schneider S, Wright CM, and Heuckeroth RO. Unexpected Roles for the Second Brain: Enteric Nervous System as Master Regulator of Bowel Function. *Annu Rev Physiol.* 2019;81:235-59.
2. Furness JB. The enteric nervous system and neurogastroenterology. *Nat Rev Gastroenterol Hepatol.* 2012;9(5):286-94.
3. Lake JI, and Heuckeroth RO. Enteric nervous system development: migration, differentiation, and disease. *Am J Physiol Gastrointest Liver Physiol.* 2013;305(1):G1-24.
4. Uesaka T, Young HM, Pachnis V, and Enomoto H. Development of the intrinsic and extrinsic innervation of the gut. *Dev Biol.* 2016.
5. Sasselli V, Pachnis V, and Burns AJ. The enteric nervous system. *Dev Biol.* 2012;366(1):64-73.
6. Avetisyan M, Schill EM, and Heuckeroth RO. Building a second brain in the bowel. *J Clin Invest.* 2015;125(3):899-907.
7. Burns AJ, and Le Douarin NM. The sacral neural crest contributes neurons and glia to the post-umbilical gut: spatiotemporal analysis of the development of the enteric nervous system. *Development.* 1998;125:4335-47.
8. Yu Q, Du M, Zhang W, Li L, Gao Z, Chen W, et al. Mesenteric neural crest cells are the embryological basis of skip segment Hirschsprung's disease. *Cell Mol Gastroenterol Hepatol.* 2020.
9. Espinosa-Medina I, Jevans B, Boismoreau F, Chettouh Z, Enomoto H, Muller T, et al. Dual origin of enteric neurons in vagal Schwann cell precursors and the sympathetic neural crest. *Proc Natl Acad Sci U S A.* 2017;114(45):11980-5.
10. Uesaka T, Nagashimada M, and Enomoto H. Neuronal Differentiation in Schwann Cell Lineage Underlies Postnatal Neurogenesis in the Enteric Nervous System. *J Neurosci.* 2015;35(27):9879-88.
11. Brokhman I, Xu J, Coles BLK, Razavi R, Engert S, Lickert H, et al. Dual embryonic origin of the mammalian enteric nervous system. *Dev Biol.* 2019;445(2):256-70.
12. Drokhlyansky E, Smillie CS, Van Wittenberghe N, Ericsson M, Griffin GK, Eraslan G, et al. The Human and Mouse Enteric Nervous System at Single-Cell Resolution. *Cell.* 2020;182(6):1606-22 e23.
13. May-Zhang AA, Tycksen E, Southard-Smith AN, Deal KK, Benthal JT, Buehler DP, et al. Combinatorial Transcriptional Profiling of Mouse and Human Enteric Neurons Identifies Shared and Disparate Subtypes In Situ. *Gastroenterology.* 2020.
14. Zeisel A, Hochgerner H, Lonnerberg P, Johnsson A, Memic F, van der Zwan J, et al. Molecular Architecture of the Mouse Nervous System. *Cell.* 2018;174(4):999-1014 e22.
15. Morarach K, Mikhailova A, Knoflach V, Memic F, Kumar R, Li W, et al. Diversification of molecularly defined myenteric neuron classes revealed by single-cell RNA sequencing. *Nat Neurosci.* 2021;24(1):34-46.
16. Memic F, Knoflach V, Morarach K, Sadler R, Laranjeira C, Hjerling-Leffler J, et al. Transcription and Signaling Regulators in Developing Neuronal Subtypes of Mouse and Human Enteric Nervous System. *Gastroenterology.* 2018;154(3):624-36.
17. Wright CM, Schneider S, Smith-Edwards KM, Mafra F, Leembruggen AJL, Gonzalez MV, et al. scRNA-Seq Reveals New Enteric Nervous System Roles for GDNF, NRTN, and TBX3. *Cellular and molecular gastroenterology and hepatology.* 2021.
18. Foong JP. Postnatal Development of the Mouse Enteric Nervous System. *Adv Exp Med Biol.* 2016;891:135-43.
19. Yarandi SS, Kulkarni S, Saha M, Sylvia KE, Sears CL, and Pasricha PJ. Intestinal Bacteria Maintain Adult Enteric Nervous System and Nitrergic Neurons via Toll-like Receptor 2-induced Neurogenesis in Mice. *Gastroenterology.* 2020;159(1):200-13 e8.

20. Kulkarni S, Micci MA, Leser J, Shin C, Tang SC, Fu YY, et al. Adult enteric nervous system in health is maintained by a dynamic balance between neuronal apoptosis and neurogenesis. *Proc Natl Acad Sci U S A.* 2017;114(18):E3709-E18.
21. Uribe RA, Hong SS, and Bronner ME. Retinoic acid temporally orchestrates colonization of the gut by vagal neural crest cells. *Developmental biology.* 2018;433(1):17-32.
22. Suzuki R, Miyahara K, Murakami H, Doi T, Lane GJ, Mabuchi Y, et al. Abnormal neural crest innervation in Sox10-Venus mice with all-trans retinoic acid-induced anorectal malformations. *Pediatr Surg Int.* 2014;30(2):189-95.
23. Gisser JM, Cohen AR, Yin H, and Gariepy CE. A novel bidirectional interaction between endothelin-3 and retinoic acid in rat enteric nervous system precursors. *PLoS One.* 2013;8(9):e74311.
24. Simkin JE, Zhang D, Rollo BN, and Newgreen DF. Retinoic acid upregulates ret and induces chain migration and population expansion in vagal neural crest cells to colonise the embryonic gut. *PLoS One.* 2013;8(5):e64077.
25. Wright-Jin EC, Grider JR, Duester G, and Heuckeroth RO. Retinaldehyde dehydrogenase enzymes regulate colon enteric nervous system structure and function. *Dev Biol.* 2013;381(1):28-37.
26. Fu M, Sato Y, Lyons-Warren A, Zhang B, Kane MA, Napoli JL, et al. Vitamin A facilitates enteric nervous system precursor migration by reducing Pten accumulation. *Development.* 2010;137(4):631-40.
27. Sato Y, and Heuckeroth RO. Retinoic acid regulates murine enteric nervous system precursor proliferation, enhances neuronal precursor differentiation, and reduces neurite growth in vitro. *Dev Biol.* 2008;320(1):185-98.
28. Niederreither K, Vermot J, Roux IL, Schuhbaur B, Chambon P, and Dolle P. The regional pattern of retinoic acid synthesis by RALDH2 is essential for the development of posterior pharyngeal arches and the enteric nervous system. *Development.* 2003;130(11):2525-34.
29. Pitera JE, Smith VV, Woolf AS, and Milla PJ. Embryonic gut anomalies in a mouse model of retinoic Acid-induced caudal regression syndrome: delayed gut looping, rudimentary cecum, and anorectal anomalies. *Am J Pathol.* 2001;159(6):2321-9.
30. Niederreither K, Vermot J, Le Roux I, Schuhbaur B, Chambon P, and Dolle P. The regional pattern of retinoic acid synthesis by RALDH2 is essential for the development of posterior pharyngeal arches and the enteric nervous system. *Development.* 2003;130(11):2525-34.
31. Cheng B, Zhu J, Yang T, Wang S, Liu H, Wu Q, et al. Vitamin A deficiency exacerbates autism-like behaviors and abnormalities of the enteric nervous system in a valproic acid-induced rat model of autism. *Neurotoxicology.* 2020;79:184-90.
32. Frith TJR, Gogolou A, Hackland JOS, Hewitt ZA, Moore HD, Barbaric I, et al. Retinoic Acid Accelerates the Specification of Enteric Neural Progenitors from In-Vitro-Derived Neural Crest. *Stem Cell Reports.* 2020;15(3):557-65.
33. Tan M, Yang T, Liu H, Xiao L, Li C, Zhu J, et al. Maternal vitamin A deficiency impairs cholinergic and nitrergic neurons, leading to gastrointestinal dysfunction in rat offspring via RARb. *Life Sciences.* 2020;S0024-3205(20)31441-7.
34. di Masi A, Leboffe L, De Marinis E, Pagano F, Cicconi L, Rochette-Egly C, et al. Retinoic acid receptors: From molecular mechanisms to cancer therapy. *Mol Aspects Med.* 2015;41C:1-115.
35. Clarke AR, Maandag ER, van Roon M, van der Lugt NM, van der Valk M, Hooper ML, et al. Requirement for a functional Rb-1 gene in murine development. *Nature.* 1992;359(6393):328-30.
36. Rosselot C, Spraggon L, Chia I, Batourina E, Riccio P, Lu B, et al. Non-cell-autonomous retinoid signaling is crucial for renal development. *Development.* 2010;137(2):283-92.

37. Danielian PS, Muccino D, Rowitch DH, Michael SK, and McMahon AP. Modification of gene activity in mouse embryos in utero by a tamoxifen-inducible form of Cre recombinase. *Curr Biol.* 1998;8(24):1323-6.
38. Gage PJ, Rhoades W, Prucka SK, and Hjalt T. Fate maps of neural crest and mesoderm in the mammalian eye. *Investigative ophthalmology & visual science.* 2005;46(11):4200-8.
39. Lake JI, Tusheva OA, Graham BL, and Heuckeroth RO. Hirschsprung-like disease is exacerbated by reduced de novo GMP synthesis. *J Clin Invest.* 2013;123(11):4875-87.
40. Erturk A, Becker K, Jahrling N, Mauch CP, Hojer CD, Egen JG, et al. Three-dimensional imaging of solvent-cleared organs using 3DISCO. *Nat Protoc.* 2012;7(11):1983-95.
41. Schuchardt A, D'Agati V, Larsson-Blomberg L, Costantini F, and Pachnis V. Defects in the kidney and enteric nervous system of mice lacking the tyrosine kinase receptor Ret. *Nature.* 1994;367(6461):380-3.
42. Pattyn A, Morin X, Cremer H, Goridis C, and Brunet JF. The homeobox gene Phox2b is essential for the development of autonomic neural crest derivatives. *Nature.* 1999;399(6734):366-70.
43. Debbache J, Parfejevs V, and Sommer L. Cre-driver lines used for genetic fate mapping of neural crest cells in the mouse: An overview. *Genesis.* 2018;56(6-7):e23105.
44. Fu M, Landreville S, Agapova OA, Wiley LA, Shoykhet M, Harbour JW, et al. Retinoblastoma protein prevents enteric nervous system defects and intestinal pseudo-obstruction. *J Clin Invest.* 2013;123(12):5152-64.
45. Fonseca-Pereira D, Arroz-Madeira S, Rodrigues-Campos M, Barbosa IA, Domingues RG, Bento T, et al. The neurotrophic factor receptor RET drives haematopoietic stem cell survival and function. *Nature.* 2014;514(7520):98-101.
46. Canete A, Cano E, Munoz-Chapuli R, and Carmona R. Role of Vitamin A/Retinoic Acid in Regulation of Embryonic and Adult Hematopoiesis. *Nutrients.* 2017;9(2).
47. Chatterjee S, Kapoor A, Akiyama JA, Auer DR, Lee D, Gabriel S, et al. Enhancer Variants Synergistically Drive Dysfunction of a Gene Regulatory Network In Hirschsprung Disease. *Cell.* 2016;167(2):355-68 e10.
48. Tang CS, Zhuang X, Lam WY, Ngan ES, Hsu JS, Michelle YU, et al. Uncovering the genetic lesions underlying the most severe form of Hirschsprung disease by whole-genome sequencing. *Eur J Hum Genet.* 2018;26(6):818-26.
49. Damm K, Heyman RA, Umesono K, and Evans RM. Functional inhibition of retinoic acid response by dominant negative retinoic acid receptor mutants. *Proc Natl Acad Sci U S A.* 1993;90(7):2989-93.
50. Batourina E, Gim S, Bello N, Shy M, Clagett-Dame M, Shankar S, et al. Vitamin A controls epithelial/mesenchymal interactions through Ret expression. *Nature Genetics.* 2001;27:74-8.
51. Angrisano T, Sacchetti S, Natale F, Cerrato A, Pero R, Keller S, et al. Chromatin and DNA methylation dynamics during retinoic acid-induced RET gene transcriptional activation in neuroblastoma cells. *Nucleic Acids Res.* 2011;39(6):1993-2006.
52. Jiang Y, Liu MT, and Gershon MD. Netrins and DCC in the guidance of migrating neural crest-derived cells in the developing bowel and pancreas. *Dev Biol.* 2003;258(2):364-84.
53. Uesaka T, Nagashimada M, and Enomoto H. GDNF signaling levels control migration and neuronal differentiation of enteric ganglion precursors. *J Neurosci.* 2013;33(41):16372-82.
54. Hwang JY, and Zukin RS. REST, a master transcriptional regulator in neurodegenerative disease. *Curr Opin Neurobiol.* 2018;48:193-200.
55. Zhao Y, Zhu M, Yu Y, Qiu L, Zhang Y, He L, et al. Brain REST/NRSF Is Not Only a Silent Repressor but Also an Active Protector. *Mol Neurobiol.* 2017;54(1):541-50.

56. Chalazonitis A, and Kessler JA. Pleiotropic effects of the bone morphogenetic proteins on development of the enteric nervous system. *Dev Neurobiol.* 2012;72(6):843-56.
57. Chalazonitis A, Tang AA, Shang Y, Pham TD, Hsieh I, Setlik W, et al. Homeodomain interacting protein kinase 2 regulates postnatal development of enteric dopaminergic neurons and glia via BMP signaling. *J Neurosci.* 2011;31(39):13746-57.
58. Chalazonitis A, D'Autreaux F, Pham TD, Kessler JA, and Gershon MD. Bone morphogenetic proteins regulate enteric gliogenesis by modulating ErbB3 signaling. *Dev Biol.* 2011;350(1):64-79.
59. Chalazonitis A, Pham TD, Li Z, Roman D, Guha U, Gomes W, et al. Bone morphogenetic protein regulation of enteric neuronal phenotypic diversity: relationship to timing of cell cycle exit. *J Comp Neurol.* 2008;509(5):474-92.
60. Faure C, Chalazonitis A, Rheaume C, Bouchard G, Sampathkumar SG, Yarema KJ, et al. Gangliogenesis in the enteric nervous system: roles of the polysialylation of the neural cell adhesion molecule and its regulation by bone morphogenetic protein-4. *Dev Dyn.* 2007;236(1):44-59.
61. Fu M, Vohra BP, Wind D, and Heuckeroth RO. BMP signaling regulates murine enteric nervous system precursor migration, neurite fasciculation, and patterning via altered Ncam1 polysialic acid addition. *Dev Biol.* 2006;299(1):137-50.
62. Goldstein AM, Brewer KC, Doyle AM, Nagy N, and Roberts DJ. BMP signaling is necessary for neural crest cell migration and ganglion formation in the enteric nervous system. *Mech Dev.* 2005;122(6):821-33.
63. Chalazonitis A, D'Autreaux F, Guha U, Pham TD, Faure C, Chen JJ, et al. Bone morphogenetic protein-2 and -4 limit the number of enteric neurons but promote development of a TrkC-expressing neurotrophin-3-dependent subset. *J Neurosci.* 2004;24(17):4266-82.
64. Southard-Smith EM, Kos L, and Pavan WJ. Sox10 mutation disrupts neural crest development in Dom Hirschsprung mouse model. *Nat Genet.* 1998;18(1):60-4.
65. Lang D, Chen F, Milewski R, Li J, Lu MM, and Epstein JA. Pax3 is required for enteric ganglia formation and functions with Sox10 to modulate expression of c-Ret. *J Clinical Investigation.* 2000;106(8):963-71.
66. Lang D, and Epstein JA. Sox10 and Pax3 physically interact to mediate activation of a conserved c-RET enhancer. *Hum Mol Genet.* 2003;12(8):937-45.
67. Betancur P, Bronner-Fraser M, and Sauka-Spengler T. Genomic code for Sox10 activation reveals a key regulatory enhancer for cranial neural crest. *Proceedings of the National Academy of Sciences of the United States of America.* 2010;107(8):3570-5.
68. Lasrado R, Boesmans W, Kleinjung J, Pin C, Bell D, Bhaw L, et al. Lineage-dependent spatial and functional organization of the mammalian enteric nervous system. *Science.* 2017;356(6339):722-6.
69. Dickinson ME, Krumlauf R, and McMahon AP. Evidence for a mitogenic effect of Wnt-1 in the developing mammalian central nervous system. *Development.* 1994;120(6):1453-71.
70. Zechner D, Muller T, Wende H, Walther I, Taketo MM, Crenshaw EB, 3rd, et al. Bmp and Wnt/beta-catenin signals control expression of the transcription factor Olig3 and the specification of spinal cord neurons. *Developmental biology.* 2007;303(1):181-90.
71. Ciani L, and Salinas PC. WNTs in the vertebrate nervous system: from patterning to neuronal connectivity. *Nature reviews Neuroscience.* 2005;6(5):351-62.
72. Vivancos V, Chen P, Spassky N, Qian D, Dabdoub A, Kelley M, et al. Wnt activity guides facial branchiomotor neuron migration, and involves the PCP pathway and JNK and ROCK kinases. *Neural development.* 2009;4:7.
73. West KP, Jr. Extent of vitamin A deficiency among preschool children and women of reproductive age. *J Nutr.* 2002;132(9 Suppl):2857S-66S.

74. Friedrich G, and Soriano P. Promoter traps in embryonic stem cells: a genetic screen to identify and mutate developmental genes in mice. *Genes & development.* 1991;5(9):1513-23.
75. Enomoto H, Crawford PA, Gorodinsky A, Heuckeroth RO, Johnson EM, Jr., and Milbrandt J. RET signaling is essential for migration, axonal growth and axon guidance of developing sympathetic neurons. *Development.* 2001;128(20):3963-74.
76. Kilkenny C, Browne WJ, Cuthi I, Emerson M, and Altman DG. Improving bioscience research reporting: the ARRIVE guidelines for reporting animal research. *Vet Clin Pathol.* 2012;41(1):27-31.
77. Espinosa-Medina I, Saha O, Boismoreau F, Chettouh Z, Rossi F, Richardson WD, et al. The sacral autonomic outflow is sympathetic. *Science.* 2016;354(6314):893-7.
78. Grant GR, Farkas MH, Pizarro AD, Lahens NF, Schug J, Brunk BP, et al. Comparative analysis of RNA-Seq alignment algorithms and the RNA-Seq unified mapper (RUM). *Bioinformatics.* 2011;27(18):2518-28.
79. Zhou Y, Zhou B, Pache L, Chang M, Khodabakhshi AH, Tanaseichuk O, et al. Metascape provides a biologist-oriented resource for the analysis of systems-level datasets. *Nature communications.* 2019;10(1):1523.

Figures:

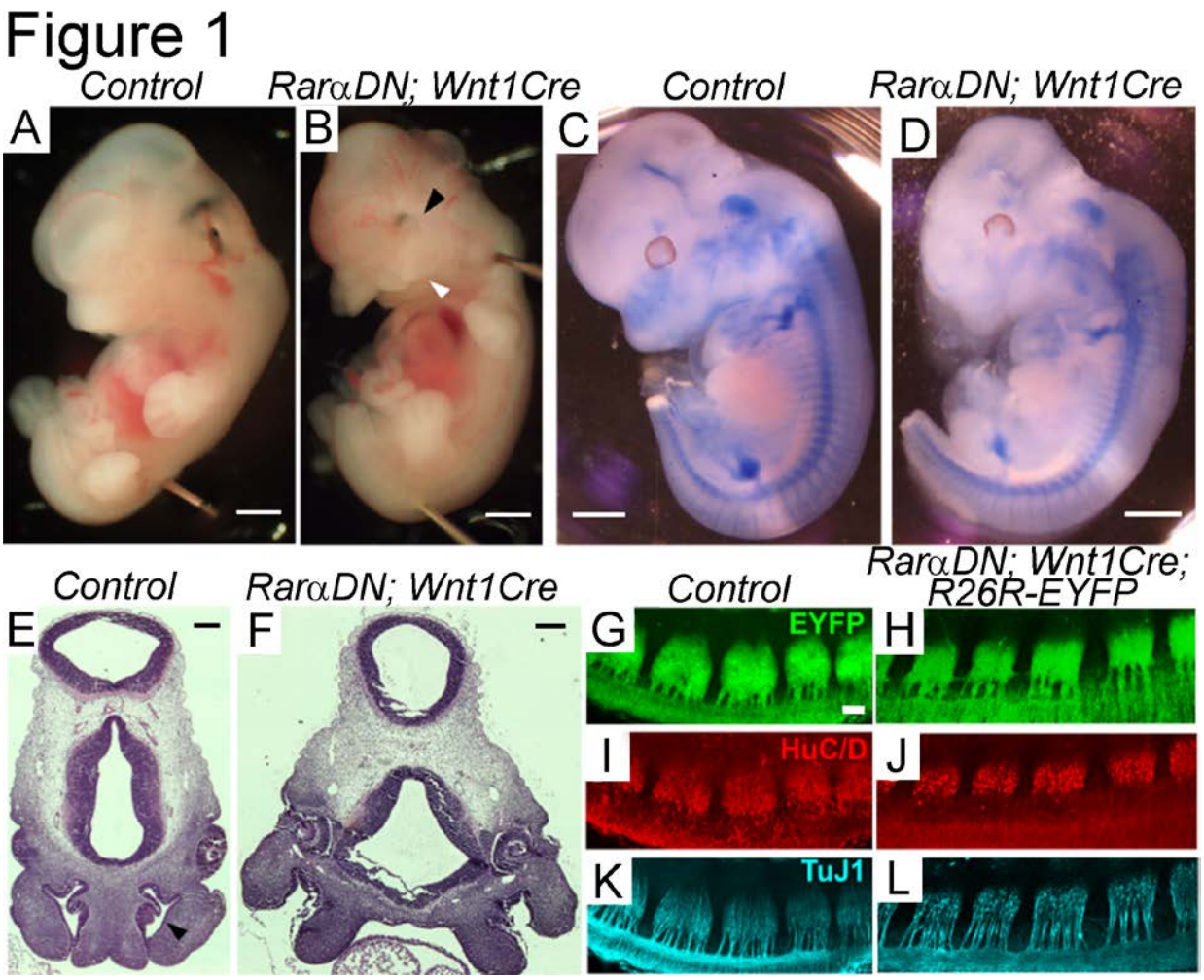

Figure 1. ***RarαDN$^{LoxP/+;}$ Wnt1Cre+ mice have abnormal craniofacial development.*** (A, B) E12.5 *RarαDN$^{LoxP/+;}$ Wnt1Cre*+ (called *RarαDN; Wnt1Cre*) mice have obvious craniofacial defects with inset eyes (black arrowhead) and midline facial cleft (white arrowhead). Scale bar = 1 mm. N=3 control, N=3 *RarαDN$^{LoxP/+}$; Wnt1Cre*+. (C, D) E12.5 Alcian blue staining shows markedly reduced cartilage in neural crest-derived structures of the face. Scale bar = 1mm. N=3 control, N=3 *RarαDN$^{LoxP/+}$; Wnt1Cre*+. (E, F) Representative images of H&E-stained coronal sections of *RarαDN$^{LoxP/+}$; Wnt1Cre*+ mice show inset eyes and cleft nasal passages compared to control (*Wnt1Cre*+) at E12.5. Arrowhead indicates nasal cavity. Scale bar = 200 μm. N=3 control, N=3 *RarαDN$^{LoxP/+}$; Wnt1Cre*+. (G-J) Dorsal root ganglia appear fairly normal at E11.5 in *RarαDN$^{LoxP/+}$;*

Wnt1Cre+; R26R-EYFP+ mice based on EYFP (G, H), HuC/D+ neuron (I, J), and TuJ1+ neurite imaging. Scale bar = 100 μm. N=3 control, N=3 *RarαDN$^{LoxP/+}$; Wnt1Cre*+.

Figure 2

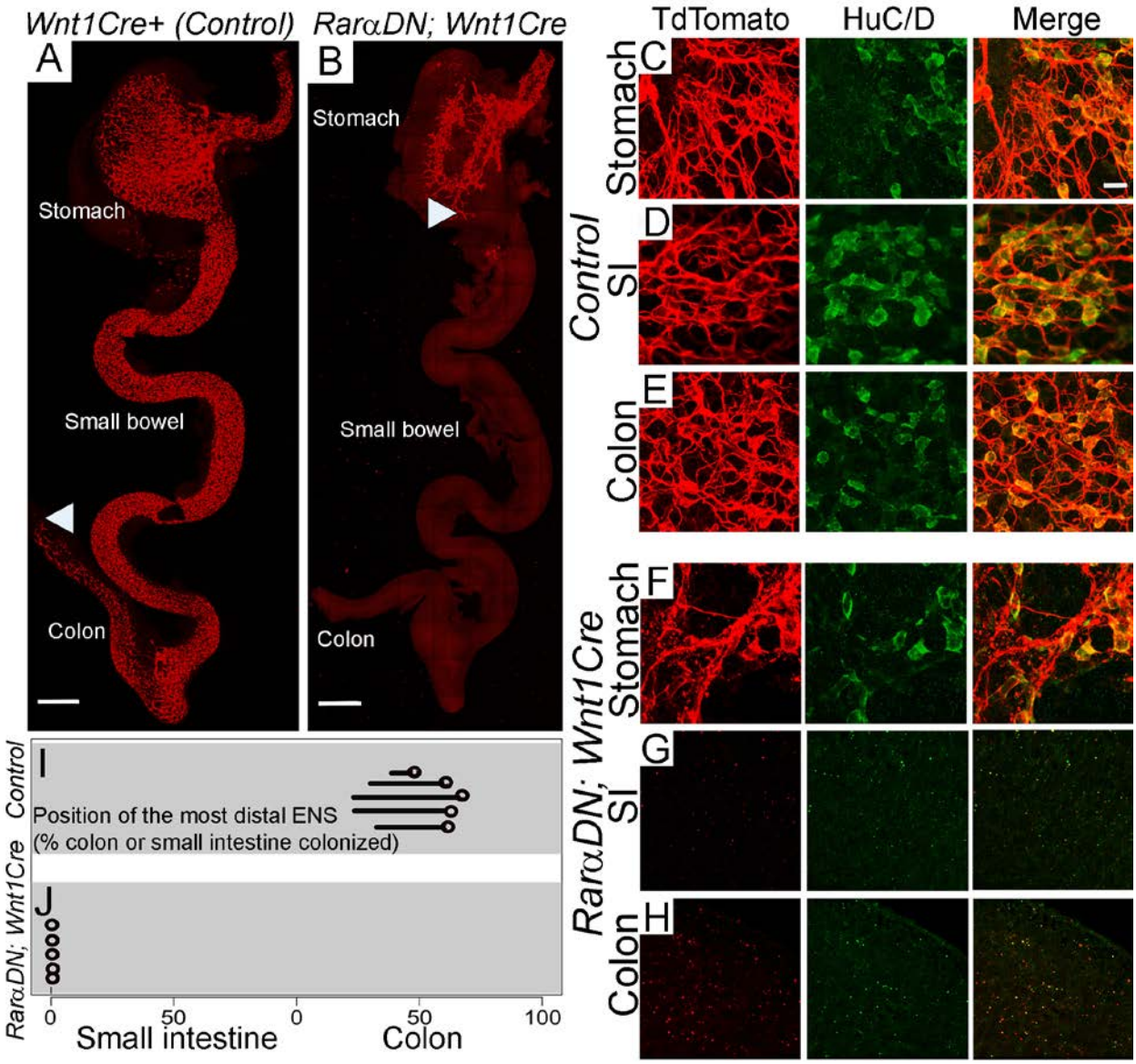

Figure 2*. Cell-autonomous RAR signaling is required for ENS precursor colonization of fetal small bowel and colon.* (A, B) Representative images of bowel colonization by TuJ1^{+} enteric neurons (red) at E12.5. (A) *Wnt1Cre*+ controls have TuJ1^{+} cells throughout the bowel from esophagus to mid-colon. (B) *RarαDN$^{LoxP/+}$; Wnt1Cre*+ mice only have TuJ1^{+} cells present in the esophagus and stomach. A white arrowhead shows the position of the most distal TuJ1+ cell or neurite in each image. Scale bars = 500 μm. (C-H) Representative E12.5 images of stomach, small intestine (SI), and colon show TdTomato+ (red) and HuC/D (green) stained cells throughout

the bowel in control (C-E), whereas TdTomato+ and HuC/D stained cells are absent in SI and colon of *RarαDN$^{LoxP/+}$; Wnt1Cre*+ mice (F-H). (C-H) Scale bar = 150 μm. (I-J) Circles show the position of the most distal TdTomato+ ENS cell in control or *RarαDN$^{LoxP/+}$; Wnt1Cre*+ mice at E12.5. The line attached to each circle indicates a hypoganglionic zone in controls. N=5 controls, N=5 *RarαDN$^{LoxP/+}$; Wnt1Cre*+.

Figure 3

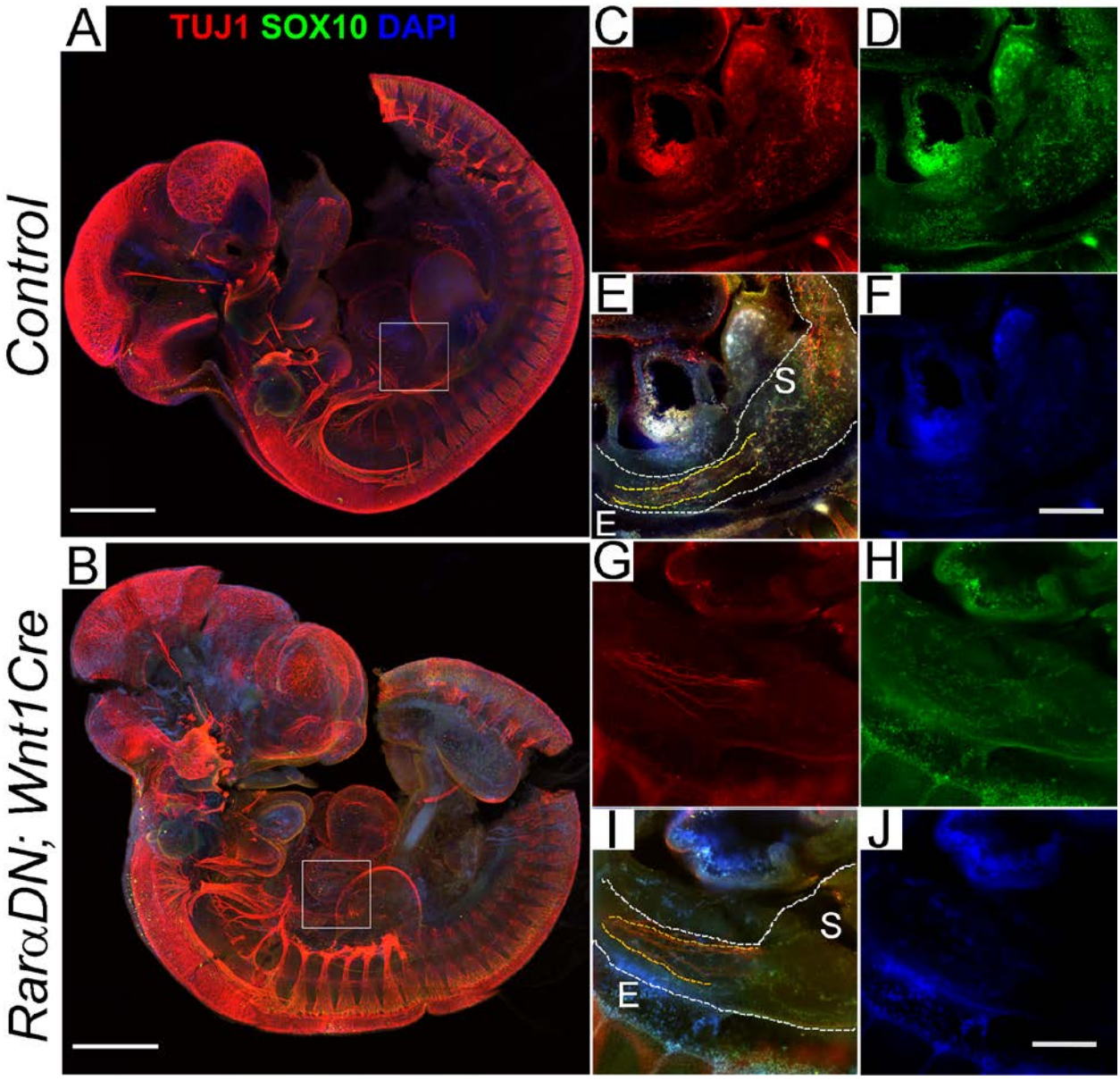

Figure 3. ***Blocking RA signaling impairs ENCDC migration and differentiation at E10.5.*** (A, B) Whole embryo imaging showing E10.5 *RarαDN*$^{LoxP/+}$ (control) (A) or E10.5 *RarαDN*$^{LoxP/+}$*; Wnt1Cre*+ (B) mice stained with TUJ1 (red) and SOX10 (green) antibodies plus DAPI (blue). Scale bar = 500 μm. (C-J) Zoomed in images of selected slices from the Z-stack of the whole embryos show esophagus and stomach from control (C-F) or *RarαDN*$^{LoxP/+}$*; Wnt1Cre*+ (G-J) mice. Scale bar = 100 μm. In control embryos, there are readily visible SOX10^{+}TUJ1^{+} cells in both

esophagus and stomach area (C, D, E, F). In contrast, there are almost no SOX10^{+} cells in the mutant stomach, even though SOX10^{+} cells were observed in the esophagus (G, H, I, J). (E, I). White dotted lines outline of esophagus and stomach. Yellow dotted lines highlight the region with extrinsic vagal nerve fibers. E = Esophagus. S = Stomach. These are representative images from N=3 *RarαDN$^{LoxP/+}$* (control), N=3 *RarαDN$^{LoxP/+}$; Wnt1Cre*+.

Figure 4

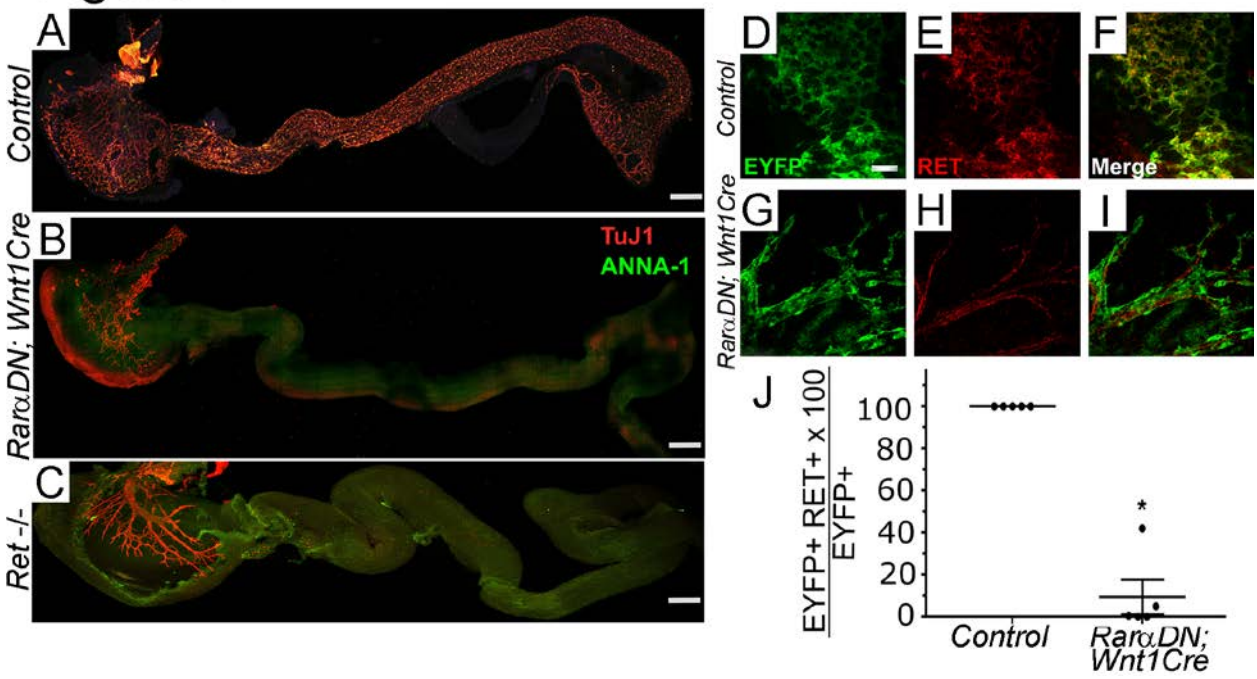

Figure 4. ***RA signaling in ENCDC is required for Ret expression*** (A-C) Whole mount TuJ1 and HuC/D antibody staining of E12.5 bowel from control, *RarαDN$^{LoxP/+}$;Wnt1Cre+*, *and Ret-/-* mice. Note that there are no ENCDC beyond stomach in *RarαDN$^{LoxP/+}$; Wnt1Cre+* (B) or *Ret-/-* mice (C). Scale bar = 1000 μm. (D-I) Immunohistochemistry of E12.5 Control (*Wnt1Cre+; Rosa26^{EYFP}*) (D, E, F) or *RarαDN$^{LoxP/+}$; Wnt1Cre+; Rosa26^{EYFP}* (G, H, I) stomach using EYFP and RET antibodies. Scale bar = 50 μm. (J) Percentage ratio of EYFP^{+} ENCDC that are RET immunoreactive. *Wnt1Cre+; Rosa26^{EYFP}* (N=5 mice, 2100 cells), *RarαDN$^{LoxP/+}$; Wnt1Cre+; Rosa26^{EYFP}* (N=5 mice, 1994 cells, P = 0.0002, 2-tailed unpaired Student's t-test).

Figure 5

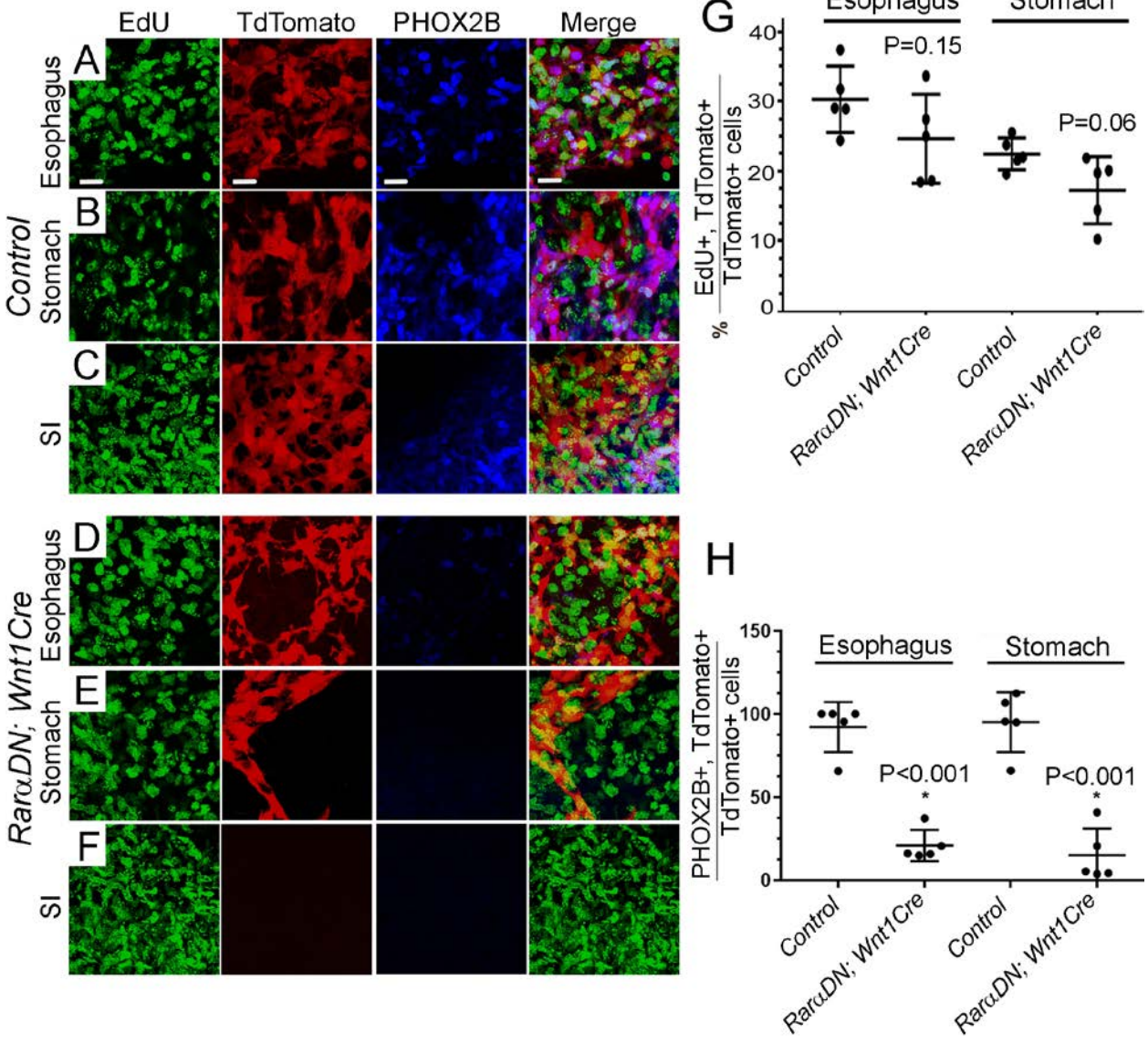

Figure 5. ***RAR signaling in ENCDC is required for Phox2b expression*** (A-F) *Wnt1Cre+; R26R-TdTomato* (Control) and *RarαDN$^{LoxP/+}$; Wnt1Cre+; R26R-TdTomato* E12.5 bowel whole-mount showing EdU and PHOX2B immunohistochemistry as well as TdTomato fluorescence in esophagus (A, D), stomach (B, E), and small intestines (C, F). (G) Cell proliferation rate (EdU$^+$TdTomato$^+$/TdTomato$^+$ x 100) (N=5 mice, 718 cells) was similar in *Wnt1Cre+; R26R-TdTomato* (control) and *RarαDN$^{LoxP/+}$; Wnt1Cre+* mice*; R26R-TdTomato* (N=5 mice, 643 cells). Unpaired Student's t-tests were used for statistics. (H). Quantitative analysis of PHOX2B

expression in ENCDC (PHOX2B^{+}TdTomato^{+}/TdTomato^{+} x 100) showed few mutant ENCDC are PHOX2B+. *Wnt1Cre+; R26R-TdTomato* (Control) (N=5 mice, 718 cells); *RarαDN$^{LoxP/+}$; Wnt1Cre+; R26R-TdTomato* (N=5 mice, 643 cells). Scale bar = 20 μm. 2-tailed unpaired student's t-tests were used for statistics.

Figure 6

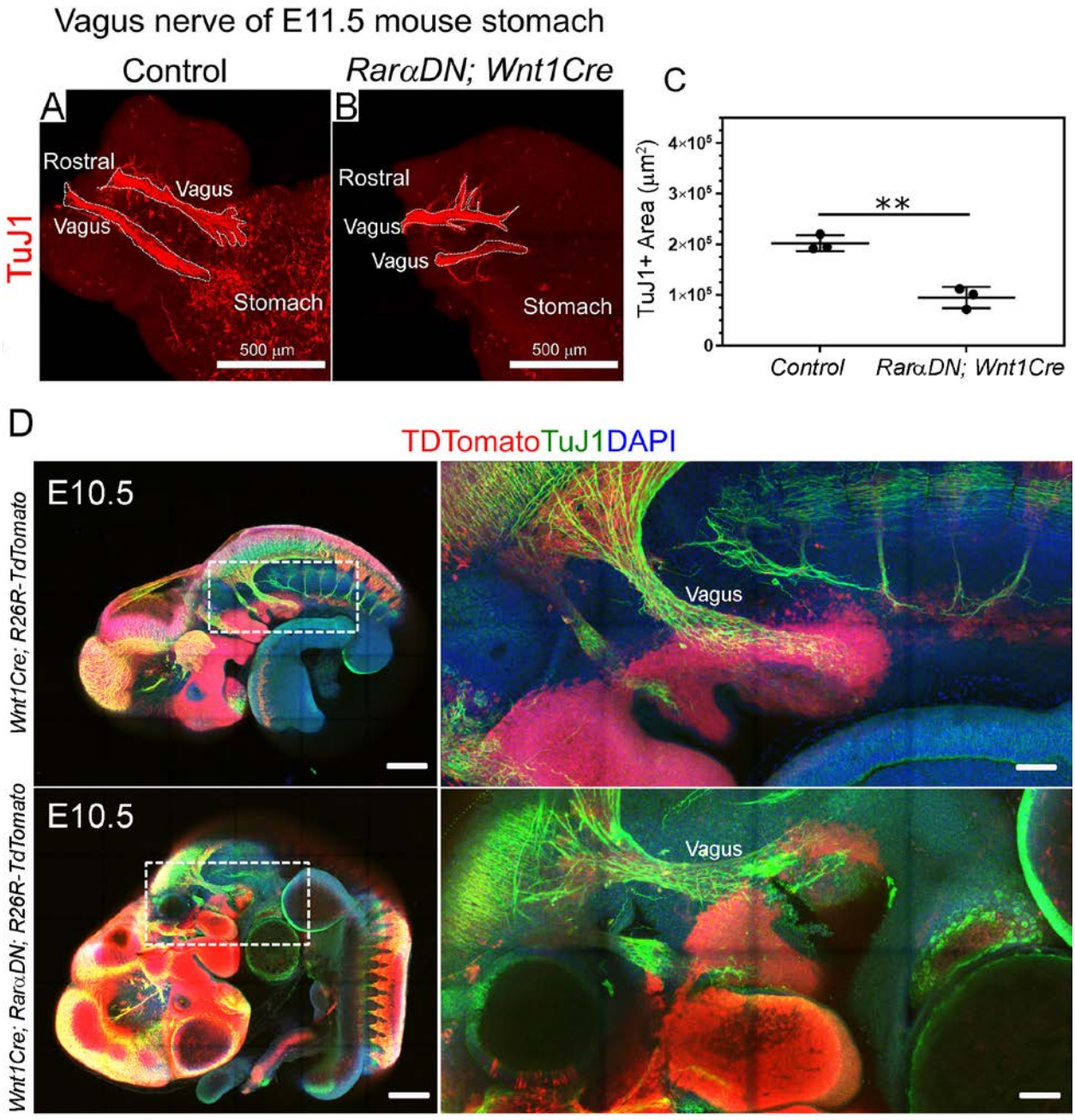

Figure 6. Vagal nerve fibers occupy a smaller area in E11.5 stomach of *RarαDN$^{LoxP/+}$; Wnt1Cre+* mice than in controls. TuJ1 antibody-stained E11.5 stomach of *RarαDN$^{LoxP/+}$* (control) (A) or *RarαDN$^{LoxP/+}$; Wnt1Cre+* (B) mice. Scale bar = 500 μm. (C) Quantification of TuJ1^{+} stained vagal fiber area. ** $P < 0.01$, 2 tailed unpaired Student's t-tests were used for statistics. (D) Whole embryo imaging of E10.5 *Wnt1Cre+; R26R-TdTomato+* and *RarαDN$^{LoxP/+}$; Wnt1Cre+;*

R26R-TdTomato+. Scale bars = 500 μm (left) and 200 μm (right, enlarged). Note that TuJ1+ vagal nerve fibers are not TdTomato+. Box shows region of the magnified image. N=3, *Wnt1Cre+; R26R-TdTomato*+; N=3, *RarαDN$^{LoxP/+}$; Wnt1Cre+; R26R-TdTomato*+. Supplemental Videos 1 and Supplemental Video 2 show three-dimensional Z-stacks from embryos in Figure 6D.

Figure 7

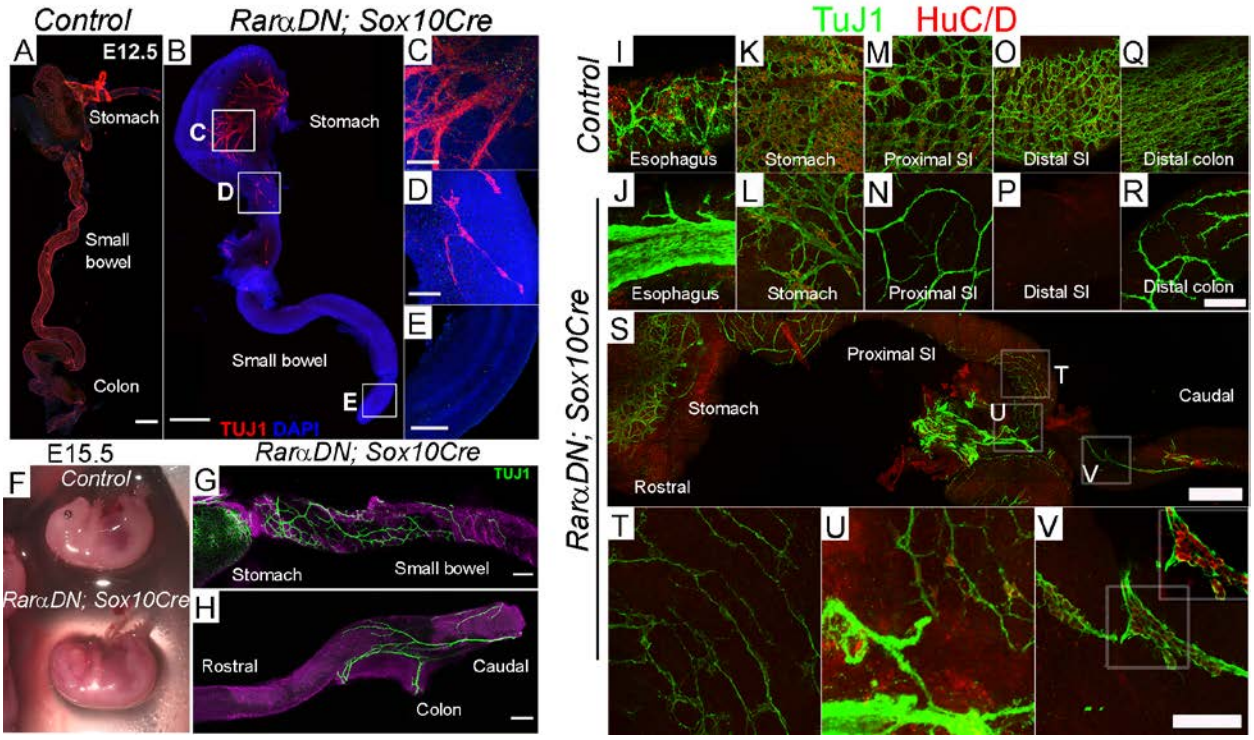

Figure 7. *RarαDN$^{LoxP/+}$; Sox10Cre+ mice had extensive distal bowel aganglionosis.* (A-E) E12.5 control or *RarαDN$^{LoxP/+}$; Sox10Cre*+ whole bowel was stained with TuJ1 antibody (red) and DAPI (blue). Insets highlight mutant stomach (inset C), proximal small intestine (inset D), and distal small intestine (inset E). Sparse TuJ1^{+} nerve cell bodies were seen in the proximal small bowel (D), but not in more distal small bowel (E) of *RarαDN$^{LoxP/+}$; Sox10Cre*+ mice. (A, B) Scale bars = 500 μm. (C-F) and 100 μm. (F) Images of either *RarαDN$^{LoxP/+}$* (control) or *RarαDN$^{LoxP/+}$; Sox10Cre*+ E15.5 embryos. Note the defective eye and craniofacial development of the mutant embryos. (G, H) E15.5 *RarαDN$^{LoxP/+}$; Sox10Cre*+ bowels were stained with TuJ1 (green) and counter-stained with DAPI. Note the TuJ1+ network at proximal small intestine (G) and distal colon (H). Scale bars = 100 μm. (I-R) *RarαDN$^{LoxP/+}$* (Control) or *RarαDN$^{LoxP/+}$; Sox10Cre*+ bowels were stained with HuC/D (red) and TuJ1 (green) antibodies. Representative images of esophagus (I, J), stomach (K, L), proximal small intestine (M, N), distal small intestine (O, P), and end of distal colon (Q, R). Scale bar = 50 μm. (S) Proximal small intestine of E15.5 *RarαDN$^{LoxP/+}$; Sox10Cre*+

bowel. Regions outlined by boxes indicate which areas are enlarged in (T-V). Note extrinsic nerve fibers (S regions T, U). (S) Scale bar = 500 μm. (T-V) Scale bar = 50 μm. N=3, *RarαDN$^{LoxP/+}$* (Control); N=3, *RarαDN$^{LoxP/+}$; Sox10Cre+.*

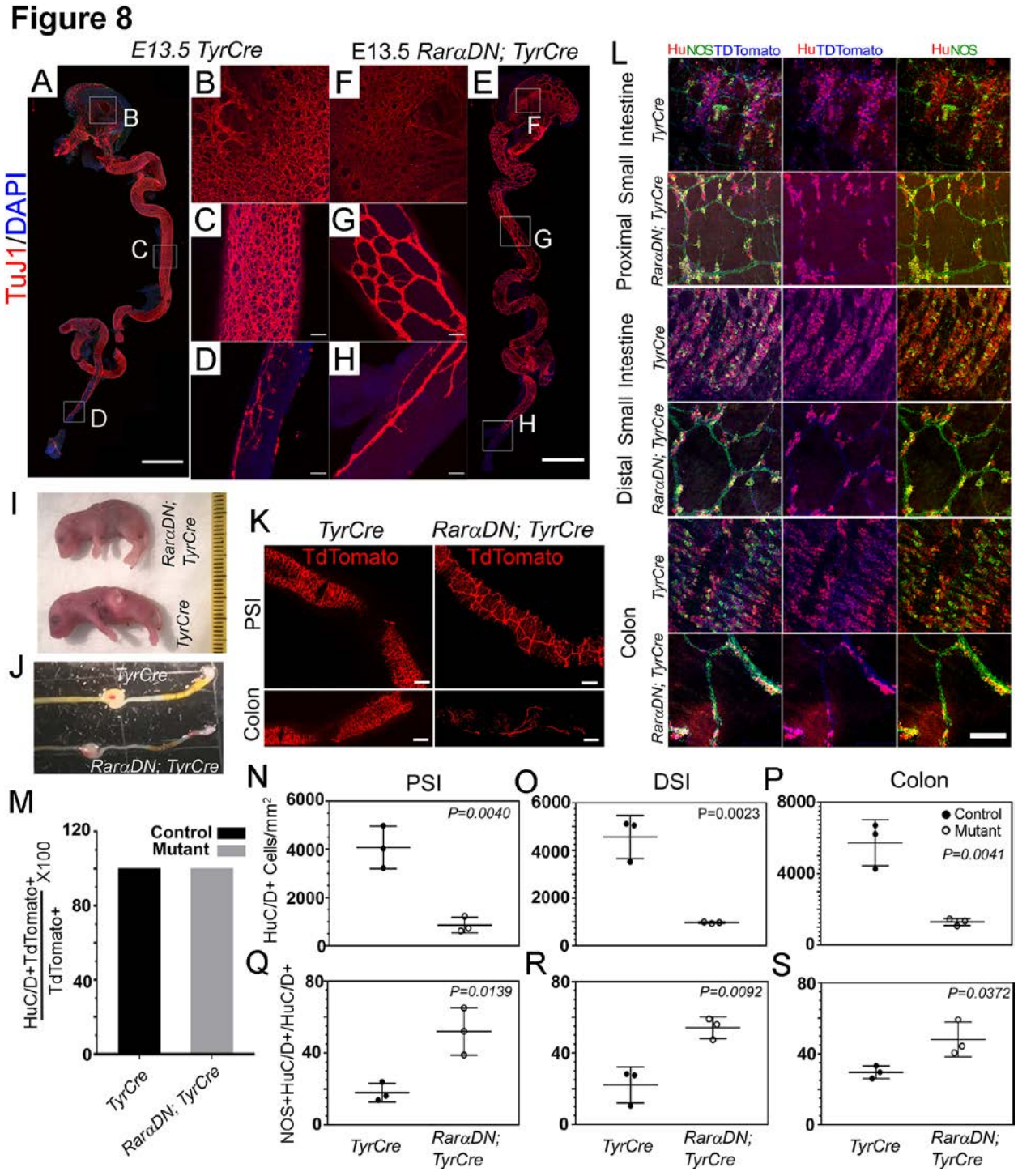

Figure 8. ***TyrCre-driven RarαDN reduces enteric neuron number and causes abnormal ENS patterning.*** (A-H) E13.5 *RarαDN$^{LoxP/+}$; TyrCre+* or *TyrCre+* (control) bowels stained with TuJ1 antibody (red) and DAPI. (A, E) Scale bars = 1 mm. Boxes in (A) and (E) indicate regions of stomach (B, F), midgut (C, G), and distal colon (D, H) that are magnified in adjacent images. (B-

H) Scale bars = 50 μm. (I) *RarαDN$^{LoxP/+}$; TyrCre*+ appear similar to control (*TyrCre+)* at birth, but did not feed and lack a milk spot in stomach (n = 6). (J) *RarαDN$^{LoxP/+}$; TyrCre*+ distal bowel appeared grossly similar to control (*TyrCre*+) at P0 (n = 10) (K) TdTomato+ images of proximal small intestine (PSI) and colon of either *RarαDN$^{LoxP/+}$; TyrCre*+ or *TyrCre*+ (control) E18.5 pups. Scale bar = 1 mm. (L) Whole mount immunohistochemistry of E18.5 *RarαDN$^{LoxP/+}$; TyrCre*+ or *TyrCre*+ (control) bowels using HuC/D (red), NOS1 (green) antibodies and via TdTomato (blue) fluorescence. Scale bar = 100 μm. (M) All TdTomato+ cells in small bowel and colon were HuC/D+ in E18.5 *RarαDN$^{LoxP/+}$; TyrCre*+ and *TyrCre*+ (control) mice. (N-S) Total HuC/D+ neurons were reduced in PSI, distal small intestine (DSI) and colon of *RarαDN$^{LoxP/+}$; TyrCre*+ mice (N-P), but the percentage of HuC/D+ neurons expressing NOS1 was increased in mutants (Q-S). N=3, *TyrCre*+ (Control); N=3, *RarαDN$^{LoxP/+}$; TyrCre*+. 2-tailed unpaired student's t-tests were used for statistics.

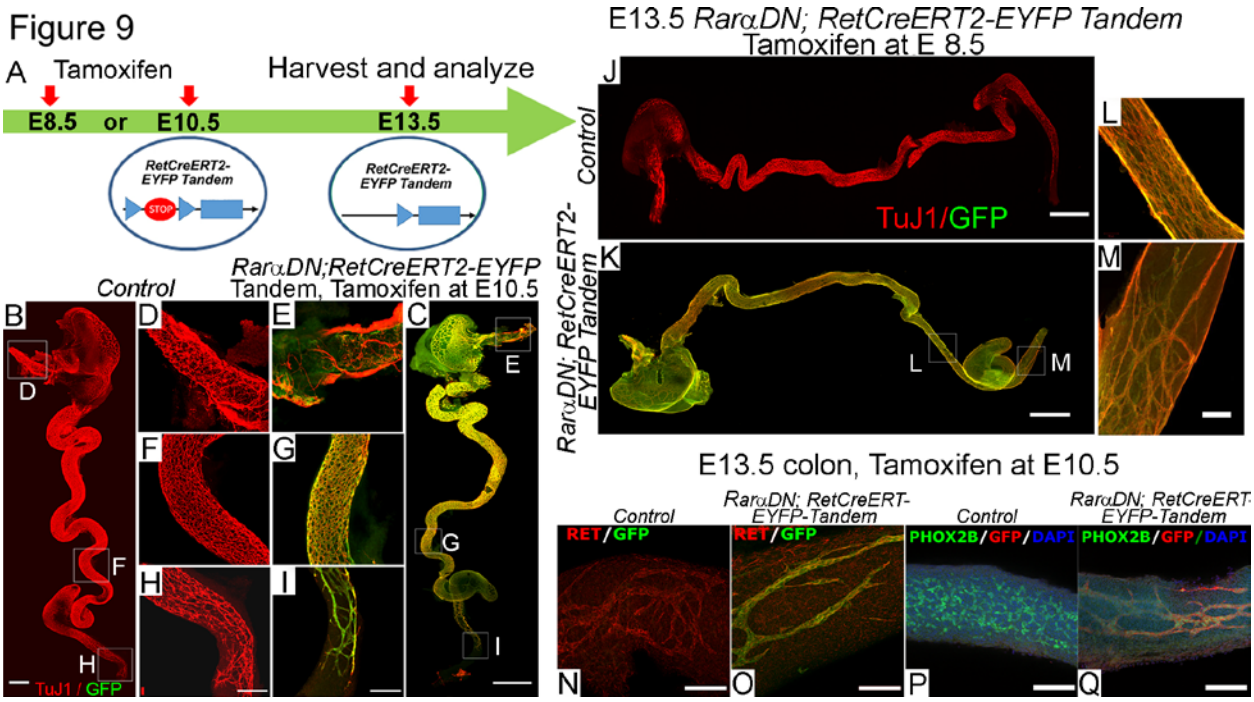

Figure 9. ***Inactivation of RAR signaling in Ret lineage at E8.5 or E10.5*** (A) *RarαDN$^{LoxP/+}$; RETCreERT2-EYFP^{Tandem}* have *CreERT2* knocked into the *Ret* locus and *Channelrhodopsin-2 (ChR2)-Lox-Stop-Lox-EYFP* in the nearby *Rosa26* locus on the same chromosome. Tamoxifen activates CreERT2 to induce expression of *RarαDN* and *EYFP*. E13.5 whole bowel from (B) Control (*RarαDN$^{LoxP/+}$* that lacks *RETCreERT2-EYFP^{Tandem}*) or (C) *RarαDN$^{LoxP/+}$; RETCreERT2-EYFP^{Tandem}* after E10.5 tamoxifen treatment. ENS was visualized using TuJ1 (red) and GFP (green) antibodies. Boxes indicate regions of esophagus (D, E), small bowel (F, G) and distal colon (H, I) that are magnified in adjacent images. (B, C) Scale bar = 1000 μm. Magnified images (D-I) scale bar = 500 μm. (J, K) E13.5 bowel after E8.5 tamoxifen treatment. Scale bar = 1000 μm. (K) Boxes labeled L and M indicate regions of magnified images (L, M) from *RarαDN$^{LoxP/+}$; RETCreERT2-EYFP^{Tandem}* small bowel (L) or distal colon (M). Magnified image scale bar = 100 μm. (N, O) RET (red) and GFP (green) antibody stained E13.5 colon after E10.5 tamoxifen treatment. (P, Q) PHOX2B (green), GFP (red) and DAPI (blue) stained E13.5 colon after E10.5 tamoxifen treatment. Scale bar = 100 μm. N=3 in each group.

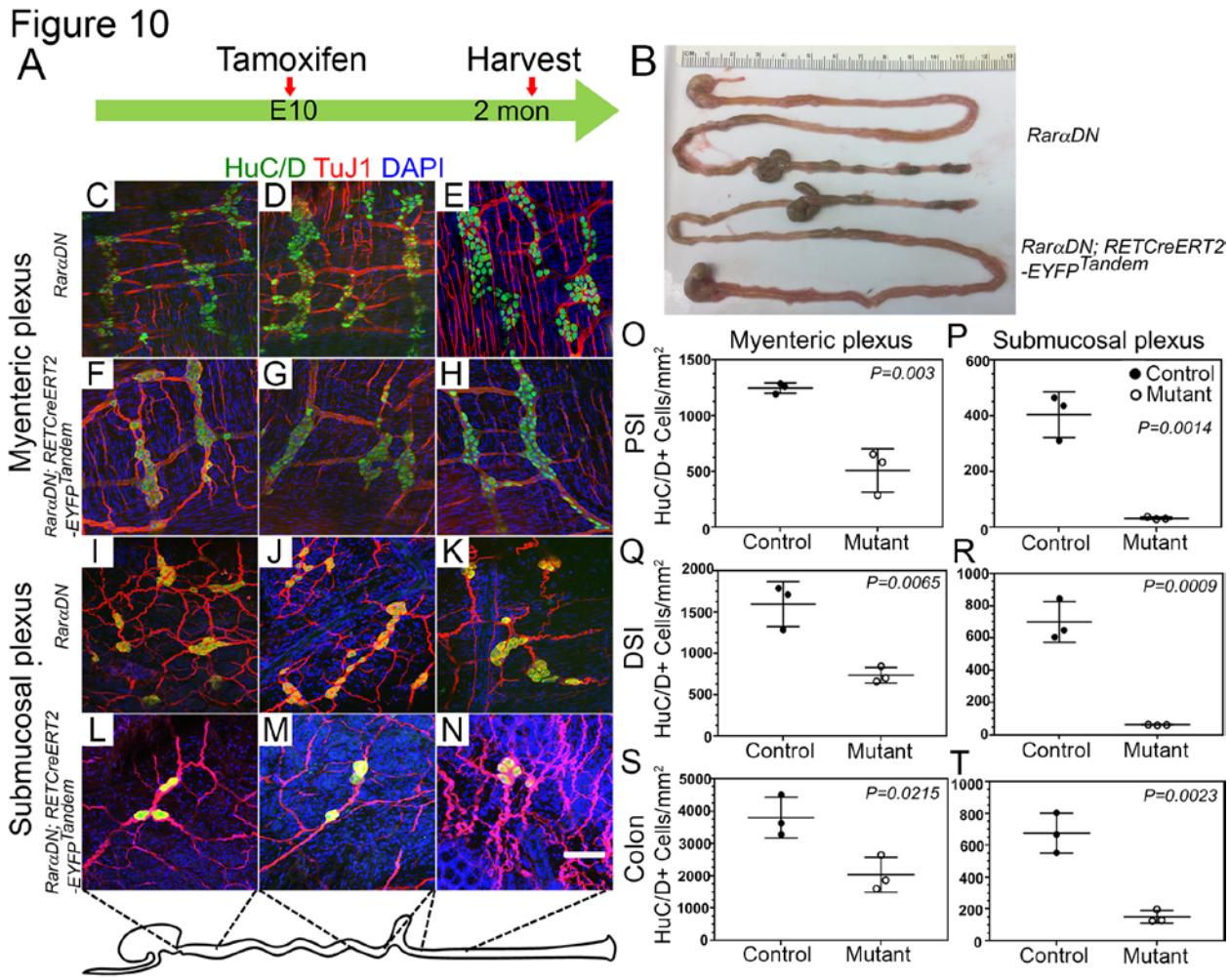

Figure 10. Postnatal ENS phenotype when RAR signaling is inactivated in *Ret* lineage starting from E10.5 (A) Tamoxifen was given to pregnant mice at E10.5 to activate the *RarαDN* transgene and bowel was harvested at ~2 months of age. (B) *RarαDN*$^{LoxP/+}$ (control) or *RarαDN*$^{LoxP/+}$*; RETCreERT2-EYFP*^{Tandem} (mutant) bowels appear similar. (C-N) Myenteric and submucosal plexus in *RarαDN*$^{LoxP/+}$ (control) or *RarαDN*$^{LoxP/+}$*; RETCreERT2-EYFP*^{Tandem} (mutant) animals were visualized in whole mounts using HuC/D (green) and TuJ1 (red) antibodies plus DAPI (blue). Scale bar = 100 μm. (O-T) Quantification of HuC/D positive neurons shows ~50% fewer myenteric and ~90% fewer submucosal neurons in *RarαDN-RETCreERt2-EYFP*^{Tandem} (mutant) animals compared to *RarαDN*$^{LoxP/+}$ (control) (n=3 in each group). 2-tailed unpaired student's t-tests were used for statistics.

Figure 11

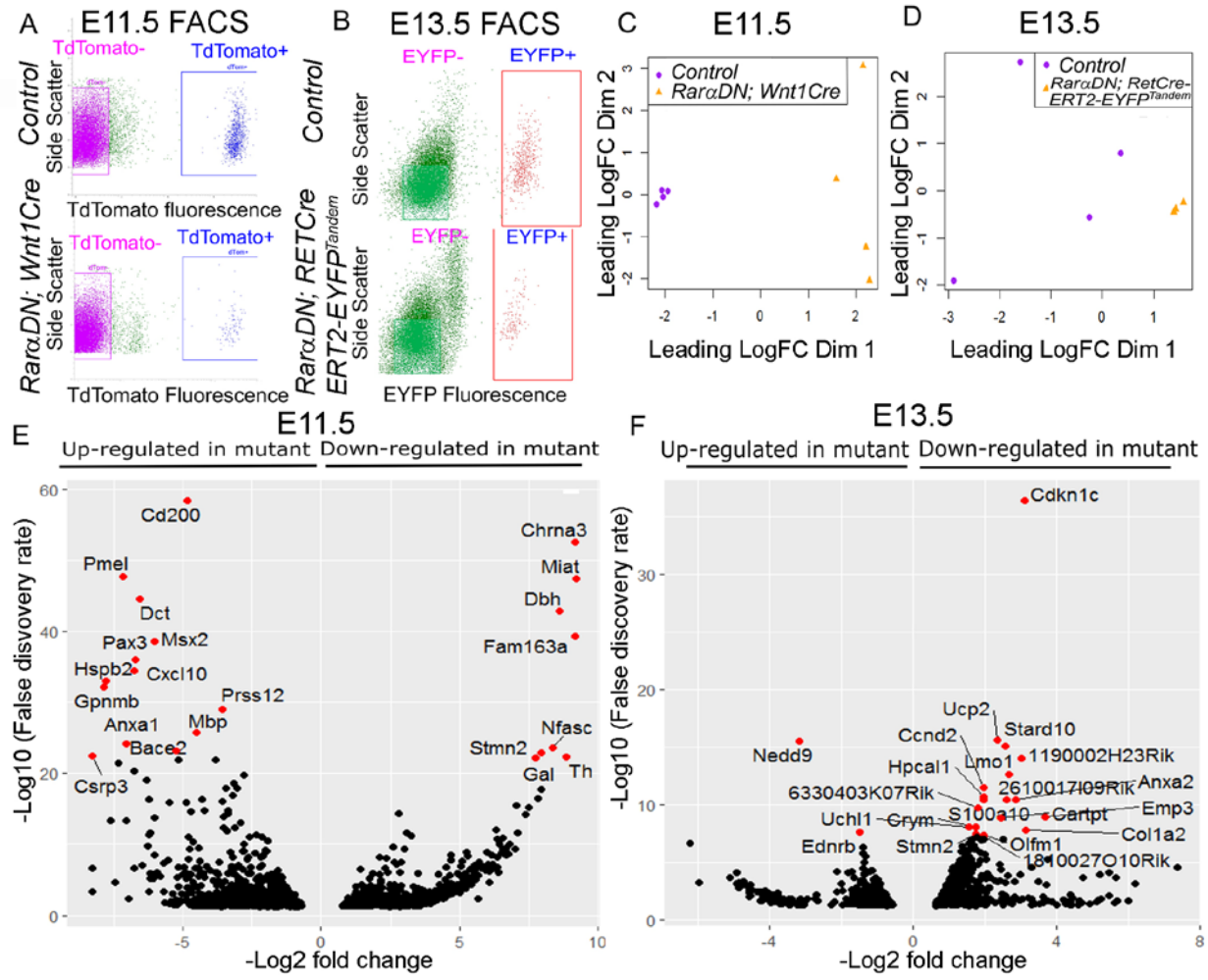

Figure 11. ***RNAseq shows many genes are dysregulated after RaraDN expression in the ENS.*** (A) ENCDC were isolated from E11.5 stomach of *RaraDN$^{LoxP/+}$; Wnt1Cre+; R26R-TdTomato* and *Wnt1Cre+; R26R-TdTomato* (control) mice based on TdTomato Fluorescence (n=4 each). (B) ENCDC were isolated from E13.5 colon of *RaraDN$^{LoxP/+}$; RETCreERT2-EYFP^{Tandem}* or *RETCreERT2-EYFP^{Tandem}* (control) mice based on EYFP-fluorescence after tamoxifen treatment at E10.5 (n=4 each, but one *RaraDN$^{LoxP/+}$; RETCreERT2-EYFP^{Tandem}* failed quality control leaving n=3 for this genotype). (C, D) Multidimensional Scaling analysis (MDS) of RNAseq data. (E, F) Volcano plots show differentially expressed genes.

Figure 12

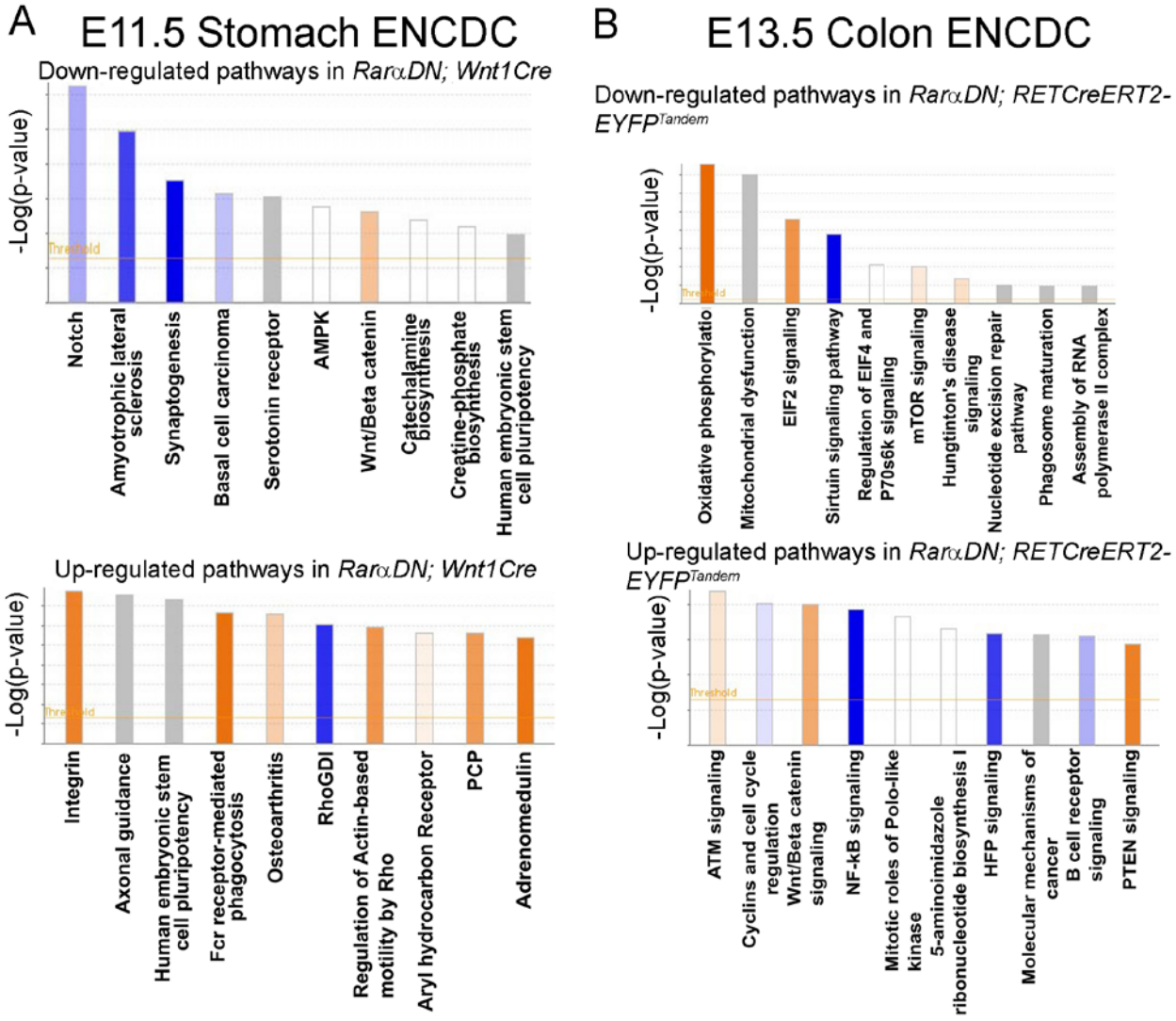

Figure 12. Pathway analysis for genes dysregulated by RARαDN. Ingenuity Pathway Analysis (IPA) of differentially expressed genes (FDR <0.05) at E11.5 (A) and E13.5 (B).

Table 1. *RarαDN$^{LoxP/+}$; Wnt1Cre+* embryos obtained at various ages. Embryo loss occurs between E12.5 and E14.5.

Age	Litters analyzed	Total embryos analyzed	Expected *RarαDN*; Wnt1Cre number	Actual *RarαDN; Wnt1Cre* number	Chi-Square statistic	p value
E10.5	5	41	10.25	10	0.004	0.949571
E11.5	14	109	27.25	37	2.098	0.147492
E12.5	22	147	36.75	26	2.341	0.126009
E14.5	5	34	8.5	0	11.333	0.0008